# Last Glacial d$^{13}$C Distribution and Deep-Sea Circulation in the Atlantic Ocean: A Model - Data Comparison

M. Matthies*, T. Bickert and A. Paul

*Universität Bremen, Fachbereich Geowissenschaften, Klagenfurter Straße, 28334 Bremen, Germany*
** corresponding author (e-mail): mmat@palmod.uni-bremen.de*

**Abstract:** We used a carbon cycle model (HAMOCC2) coupled to a general ocean circulation model (LSG) to explore the $\delta^{13}C$ distribution in the glacial Atlantic Ocean. We compared the simulated $\delta^{13}C$ pattern with a new data set of benthic carbon isotopes of the Western and Eastern Atlantic from the Last Glacial Maximum (18,000 to 20,000 $^{14}C$ years or 21,000 - 23,500 calendar years before present). The model output fits the $\delta^{13}C$ distribution derived from sediment samples, when the glacial export of NADW to the Southern Ocean was reduced by 50 % and the inflow of glacial AABW was held constant. In most cases, the modeled $\delta^{13}C$ pattern matched the paleodata within a range of ±0.2 ‰. Furthermore, the asymmetry between the glacial NADW distribution in the South Atlantic basins was reproduced by the coupled ocean circulation and carbon cycle models. No additional increase of the nutrient inventory in the deep ocean was necessary to reproduce the paleodata. Hence we conclude that a significant increase in biological pumping during glacials may not be necessary to explain the reconstructed $\delta^{13}C$ distribution in this region. The results are discussed with respect to other scenarios for the decrease of global atmospheric $pCO_2$.

## Introduction

The partial pressure of atmospheric carbon dioxide ($pCO_2$) in the in the Last Glacial Maximum (LGM), about 21,000 years ago is estimated to about 200 ppm, about 80 ppm less compared to the preindustrial value. The cause of this variation in carbon dioxide ($CO_2$) has not yet been identified (Broecker and Henderson 1998; Archer et al. 2000a; Sigman and Boyle 2000). In the recent literature, there are many hypotheses trying to explain this strong reduction in atmospheric $pCO_2$. These hypotheses involve changes in the nutrient inventory, in the oceanic pH, in the ocean circulation, or a combination of these factors.

### *Biological Pump Scenarios*

One group of mechanisms to lower the glacial $pCO_2$ is to increase the rate of biological productivity in the surface ocean, whereby carbon is transferred from the surface ocean to the deep-sea in the form of sinking particles. Either an increase in the ocean inventory of the nutrients phosphate ($PO_4^{3-}$) and nitrate ($NO_3^-$) or a change in the ratio of nutrients to carbon in phytoplankton could have stimulated the biological pump in this way. The observation that iron availability limits phytoplankton growth in some parts of the ocean such as the Southern Ocean provides a mechanism by which the biological pump in high latitudes could have intensified in a dustier, more iron-rich glacial climate. Broecker and Henderson (1998) suggested that an enhancement of glacial iron supply to the surface ocean stimulates the rate of nitrogen fixation, causing an increase in the $NO_3^-$: $PO_4^{3-}$ ratio of the deep-sea and an increase in the effective nutrient reservoir of the ocean.

*From* WEFER G, MULITZA S, RATMEYER V (eds), 2003, *The South Atlantic in the Late Quaternary: Reconstruction of Material Budgets and Current Systems*. Springer-Verlag Berlin Heidelberg New York Tokyo, pp 695-722

### *Ocean pH Scenarios*

A second class of mechanisms to lower the glacial $pCO_2$ is to change the pH or alkalinity of the whole ocean, converting seawater $CO_2$ into bicarbonate ($HCO_3^-$) and carbonate ($CO_3^{2-}$) (e.g. Archer et al. 2000a). The pH in the ocean is controlled by the mechanism of $CaCO_3$ compensation. Any imbalance between the influx of dissolved $CaCO_3$ originating from chemical weathering on land and the removal of $CaCO_3$ by burial in the deep-sea sediments will act to change the ocean pH until the flux balance is restored. It is more difficult to preserve $CaCO_3$ in an acidic ocean. If the glacial rate of weathering were higher and the $CaCO_3$ deposition currently occurring in shallow waters were shifted to the deep-sea, or the rate of $CaCO_3$ production decreased, the $CaCO_3$ burial efficiency would increase and the ocean would become more basic. If organic carbon production increased, its degradation in sediments would also promote calcite dissolution, further increasing the pH of the ocean. $CaCO_3$ compensation may also affect the $pCO_2$ response to the biological pump scenarios described above.

### *Circulation Changes*

Toggweiler (1999) reduced the deep water ventilation in a box model that treats the boundary between mid-depth and deep water masses as a chemical barrier, separating the water with a low $CO_2$ content above from the water with high contents below. He generated reduced ventilation by decreasing the vertical exchange between deep and Antarctic surface water. This mechanism invokes only a physical process or a set of related physical processes, that stratify the interior while reducing the ventilation of the ocean's deepest water. These processes bottle up remineralised $CO_2$ at depths below 3,000 m and reduce the $CO_3^{2-}$ in the deep water in contact with most of the ocean's $CaCO_3$ sediments. Through their control of the burial of $CaCO_3$, these ventilation and stratification processes are able to drive atmospheric $CO_2$ up and down on timescales of several thousands up to ten thousand years. The mechanism works without any changes in biological activity and requires only minimal changes in the distribution of nutrients.

Another mechanism to reduce the atmospheric $CO_2$ concentration without changing productivity or alkalinity has been proposed by Stephens and Keeling (2000). They suggest that a ventilation change was driven by limitations of air-sea gas-exchange due to an increase of sea-ice in the Southern Ocean. The mechanism that is proposed to explain the observed synchronisation between Antarctic temperature and atmospheric $CO_2$ calls for dramatic changes in the structure of the deep ocean during cold periods, including a collapse of NADW formation, an expansion of the volume of the deep ocean filled with AABW, and the cooling of this deep layer virtually down to the freezing point (Keeling and Stephens 2001).

However, a study by Yu et al. (1996), based on measurements of the $^{231}Pa/^{230}Ta$ ratios in glacial and modern sediments, indicates that the export of $^{231}Pa$ from the Atlantic into the Southern Ocean continued during the LGM at roughly the modern rate. They drew the conclusion that the export of deep water formed in the North Atlantic also continued to move into the Southern Ocean at a comparable rate during the LGM. If this were true, it would falsify the hypothesized collapse of NADW formation during glacial cold periods, as first suggested by Duplessy et al. (1988) and also stated as a requirement by Keeling and Stephens (2001).

In the study presented here, we used a model-data comparison of $\delta^{13}C$ changes in the deep Atlantic, in order to test the role of deep water overturning as a main potential driving mechanism for glacial $pCO_2$ reduction. A new data set of benthic stable isotopes from sediment cores in the South Atlantic (Bickert and Mackensen this volume) allows a more detailed reconstruction of the glacial nutrient distribution in this region. We will discuss the results in view of the various hypotheses described above.

## Model Descriptions

### *Ocean General Circulation Model*

The physical ocean model used in this study is known as Hamburg Large-Scale Geostrophic Ocean Model (LSG) (Maier-Reimer et al. 1993). The glacial and modern fields of the velocity, tem-

perature, salinity and convective adjustments were derived from the global model runs of Schäfer-Neth and Paul (2001) (labeled GM for the modern and G1 for a slightly modified version of the glacial simulation) and represented the input fields for the carbon cycle model. The modifications with respect to Maier-Reimer et al. (1993) include:

- The air temperature advection has been removed. This procedure was originally used to bring the simulated North Atlantic Deep Water (NADW) production to an appropriate magnitude of the present-day climate (see Schäfer-Neth and Paul 2001).
- The advection routine for temperature and salinity is formulated in accordance with the QUICK scheme of Leonard (1979), in order to compensate for the strong reduction of NADW formation due to the neglect of air temperature advection. This scheme results in a larger fraction of newly formed NADW that flows across the equator into the South Atlantic. The price to be paid is a smaller time-step, which is about four times less than the monthly time-step used by Maier-Reimer et al. (1993) and necessitates a linear interpolation of the monthly mean sea-surface temperature and salinity.
- The sea-ice model of the original version of the LSG has not been included. Instead, the grid cells covered with sea-ice are set to the freezing point (-1.8°C). Thus the model sea-ice cover has rather been driven by monthly mean sea-surface temperatures.
- A convection scheme, which makes the water column completely stable after every time-step, has been added.
- Depth-dependent horizontal diffusivity values between 8 x $10^6$ $cm^2$ $s^{-1}$ in the top layer and 4 x $10^6$ $cm^2$ $s^{-1}$ in the bottom layer are employed. Values between 0.3 $cm^2$ $s^{-1}$ and 1.1 $cm^2$ $s^{-1}$ respectively have been assumed for the vertical diffusivity.

The forcing data for the simulations under present-day and LGM boundary conditions are specified in Table 1. The modified LSG ocean model has the same resolution, land-sea mask and bathymetry as the original model, except for the glacial experiment in which the Bering Strait is closed.

The zonally integrated meridional overturning in the modern Atlantic Ocean is shown in Figure 1, left. NADW is produced at a rate of 14 Sv, 8 Sv of which is exported across the equator to the Southern Ocean at depths below 1,500 m. There is a deep inflow of Antarctic Bottom Water (AABW) which amounts to 4 Sv. The total quantity of deep water (NADW and AABW) which flows into the Southern Ocean is 12 Sv, approximately 30 % less than the value of 18 Sv given by Schmitz (1995). The water mass boundary between NADW and AABW at a depth of 2,500 m is shallower than estimated from observations by approximately 1,500 m, which corresponds to one model layer thickness. The reason for this is probably that the newly formed NADW is too warm (1 to 2°C) above 3,000 m in the northern North Atlantic Ocean and thus not dense enough to sink to an appropriate depth. However, this is a general problem of coarse resolution models. For a detailed description see Schäfer-Neth and Paul (2001).

In the glacial Atlantic (Fig 1 b), the NADW export to the Southern Ocean is 4 Sv, a reduction of 50 % compared to the modern; the glacial NADW production amounts to 6 Sv. The inflow of glacial AABW remains unchanged at 4 Sv and the bound-

| Parameter | Present-day | LGM |
|---|---|---|
| Sea-surface temperature | Shea et al. (1990)[1] | Weinelt et al. (1996) |
| Sea-surface salinity | Levitus et al. (1994)[2] | Schäfer-Neth and Paul (2001) |
| Wind | Lorenz et al. (1996) | Lorenz et al. (1996) |

[1] Surface temperature was set to -1.8 °C over the ice covered regions from Shea et al. (1990).
[2] Winter surface salinities in the Ross and Weddell Seas are adjusted according to Johns et al. (1997).

**Table 1.** Ocean model forcing data for present-day and LGM boundary conditions.

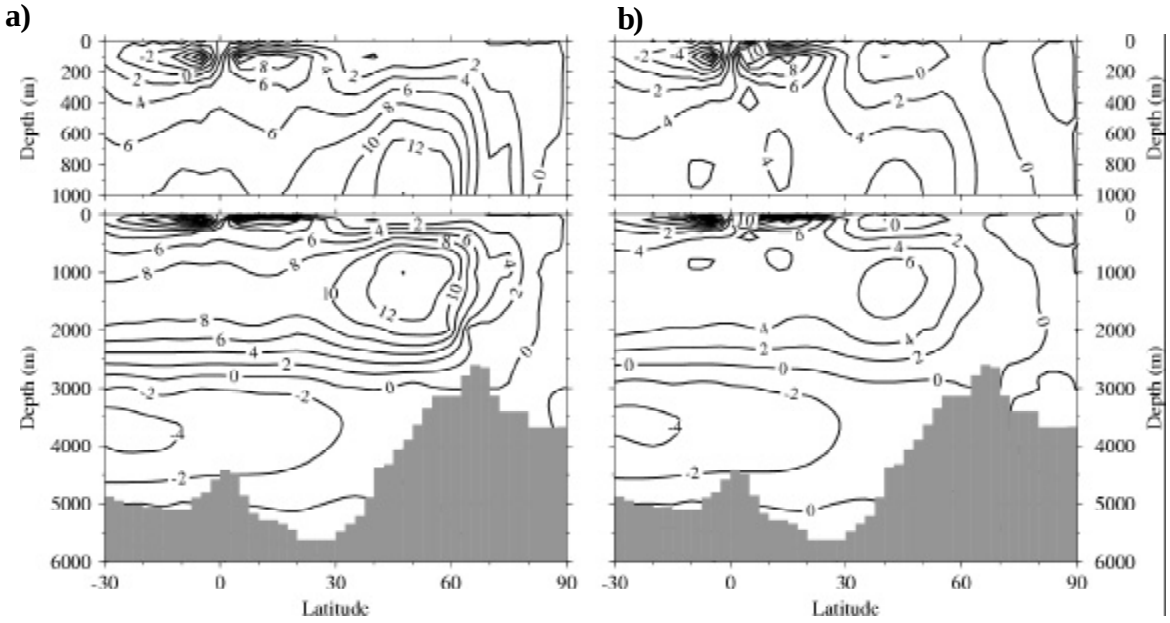


**Fig. 1.** Annual mean of zonally averaged Atlantic meridional circulation. Contour interval is 2 Sv (1 Sv = $10^6$ $m^{-3}$ $s^{-1}$). Negative contour lines indicate anti-clockwise circulation, whereas positive values indicate clockwise circulation. **a)** Simulation corresponds to the present-day boundary conditions. **b)** Simulation corresponds to the LGM boundary conditions.

ary between the Deep Current System and the Bottom Current System is only slightly shallower than in the modern ocean.

## *Carbon Cycle Model*

The model used here is the Hamburg Model of the Oceanic Carbon Cycle (HAMOCC2) (Maier-Reimer and Hasselmann 1987; Heinze et al. 1991). Only a brief outline and modifications to Heinze et al. (1991) are given in the following. The model runs on a global 72 x 72 E-grid (Arakawa and Lamb 1977), with a horizontal resolution of approximately 3.5° x 3.5° and uses 11 vertical layers with layer interfaces at 0, 50, 112.5, 200, 350, 575, 850, 1,500, 2,500, 3,500, 4,500, and 6,000 m, and has a time-step of 1 year. A quasi steady state is reached after 20,000 model years. The model tracer variables include atmospheric $pCO_2$, $\Sigma CO_2$ (total dissolved inorganic carbon), total alkalinity (including the contribution of borate), $PO_4^{3-}$ (as biolimiting nutrient), oxygen, POC (particulate organic carbon, plankton soft tissue), and particulate $CaCO_3$ (plankton calcareous shells). For all tracers that include carbon, the three carbon isotopes (the stable $^{12}C$ and $^{13}C$ and the radiocarbon $^{14}C$) were considered. The organic matter ($C_{org}$ and $C_{CaCO3}$) produced in the uppermost model layer, depending on the nutrient and light availability, is immediately redistributed within the water column because the time-step of 1 year is long relative to the time scale of sinking particulate organic matter (about 100 m $day^{-1}$, e.g. Suess 1980). The prescribed profiles for the organic carbon flux through the water column are different for POC and $CaCO_3$ and decrease exponentially with depth (with an e-folding depth of 800 and 4,000 m, respectively).

After each model run, the total inventory of $^{13}C$ was calibrated to a preanthropogenic atmospheric $\delta^{13}C$ value of -6.5 ‰, according to Friedli et al. (1986). The model configuration of Heinze et al. (1991) was modified in several respects:

• A modified profile of the vertical distribution of POC was employed. Originally, about one-third of the new production was assumed to fall immediately to the bottom layer to account for organic material coated by hard shells. This formulation was changed in such a manner that no fraction of the new production falls immediately to the bottom layer, leading to some improvements in the tracer distributions. First, this formulation yielded a greater new production (from 6.5 to 6.7 GtC $year^{-1}$) and lower $CaCO_3$ production (from 1.3 to 1.1 GtC $year^{1}$), accompanied with a corresponding decline in the atmospheric $pCO_2$ from 304 ppm to the preindustrial value of 281 ppm. Second, it reduced the models overestimation of the POC water inventory from 223 to 177 GtC $year^{-1}$ and that of the sediment pool (from 90 to 24 GtC $year^{-1}$). Third, this profile led to a better tracer distribution especially in the bottom layer of the model, where the original profile yielded an overestimation of the concentrations in the northern parts of the Atlantic and Pacific basin, as compared to the GEOSECS data. By use of this profile, the simulated $\delta^{13}C$ values in the western Atlantic basin were reduced from 0.6 to 0.4 ‰ in the source areas of the AAIW, and the water mass characteristics were more pronounced for AAIW, NADW and AABW. Consequently, a better quantitative comparison with the GEOSECS data was accomplished.

• An explicit vertical diffusion is included with the same slight depth dependency as in the ocean model (see above), to make the carbon cycle model more consistent with the ocean model. In general the vertical diffusion tends to reduce the vertical gradients, especially in the deep water column. By using the explicit vertical diffusion, the global new production increased from 6.1 to 6.7 GtC $year^{-1}$, and $CaCO_3$ production increased from 0.9 to 1.1 GtC $year^{-1}$ in the control run. The atmospheric $pCO_2$ rose from 278 to 281 ppm. This leads to advantages for some tracers, but others show a worse distribution than without explicit vertical diffusion. The advantages were most obvious in the zone of the phosphate maximum and oxygen minimum in the north and equatorial Pacific, where a consistence with GEOSECS could be reached. However, beneath this zone, the tracer values were higher in $\delta^{13}C$ and phosphate and lower in oxygen, as compared to GEOSECS. Implications of the $\delta^{13}C$ concentration in the Atlantic consisted in a small rise of 0.1 ‰ in the northern part (north of 30°N) of the bottom water, and a same enhancement in the region between 30°S and 30°N above a water depth of 800 m.

• A constant Redfield stoichiometry for POC is used, with C:N:P:O equivalent to 117:16:1:-170 according to Anderson and Sarmiento (1994).

• A rain ratio ($C_{CaCO3}$ to $C_{org}$) is prescribed which is lower than the commonly used value of 0.20 - 0.25. Here, we used a maximum rain ratio value of 0.15, following Bacastow and Maier-Reimer (1990), cf. Yamanaka and Tajika (1996). Due to this change in the rain ratio, all tracers which included $CaCO_3$ were influenced, especially the $CaCO_3$ production which is reduced from 1.7 to 1.1 GtC $year^{-1}$, if a value of 0.24 is applied. As a result, surface alkalinity and the carbonate ion concentration increased and the atmospheric $pCO_2$ decreased from 313 to 281 ppm. The effects on the $\delta^{13}C$ distribution in the Atlantic were negligible, the extension of the $\delta^{13}C$ minimum to the south was enlarged. The effect on the carbonate ion concentration was a better match of the calcite lysocline depth in the Southern Ocean with GEOSECS, and resulted in a deeper lysocline of about 400 m in this region.

The effects of these parameterisations on the model inventories and mean values are summarized in Table 2 and 3, respectively.

### *Controls on $\delta^{13}C$ of Marine Carbon*

In the marine carbon cycle, two fractionation processes are important. First, during photosynthesis, organisms preferentially take up the lighter carbon isotope $^{12}C$, increasing $\delta^{13}C$ in the surface ocean dissolved as inorganic carbon (DIC). When isotopically light organic matter is remineralised, $\delta^{13}C$ of marine $\Sigma CO_2$ decreases. This fractionation of about -20 ‰ of marine photosynthesis leaves the surface ocean depleted in nutrient with a high content of $\delta^{13}C$, whereas the nutrient-rich deep waters display low $\delta^{13}C$ values. Through this mechanism, known as biological pump, carbon and nutrients are transported to the deep-sea and thereby reduce the $CO_2$ in the surface and atmosphere.

| Inventory | Units | POC profile | No explicit vertical diffusion | Rain ratio of 0.24 | Control run |
|---|---|---|---|---|---|
| Atmospheric $pCO_2$ | Ppm | 304 | 278 | 313 | 281 |
| Total primary production | GtC/Year | 10.2 | 7.8 | 8.6 | 8.6 |
| New production | GtC/Year | 6.5 | 6.1 | 6.7 | 6.7 |
| $CaCO_3$ production | GtC/Year | 1.3 | 0.9 | 1.7 | 1.1 |
| POC ocean water pool | GtC | 223 | 174 | 177 | 177 |
| $CaCO_3$ ocean water pool | GtC | 53.2 | 52.7 | 51.1 | 53.2 |
| $\Sigma CO_2$ ocean water pool | GtC | 39494 | 39656 | 39486 | 39708 |
| Corg sediment pool | GtC | 90.0 | 22.8 | 24.3 | 24.3 |
| $CaCO_3$ sediment pool | GtC | 4029 | 4035 | 4133 | 3972 |

**Table 2.** Implications of sensitivity experiments under various model parametrisations on the tracer inventories for the modern ocean after 20,000 integrations.

| Tracer | Units | POC profile | No explicit vertical diffusion | Rain ratio of 0.24 | Control run |
|---|---|---|---|---|---|
| $\Sigma CO_2$ | µmol $kg^{-1}$ | 2250 | 2259 | 2259 | 2262 |
| Alkalinity | µequiv $kg^{-1}$ | 2367 | 2366 | 2355 | 2373 |
| Phosphate | µmol $kg^{-1}$ | 2.03 | 2.09 | 2.09 | 2.09 |
| Oxygen | µmol $kg^{-1}$ | 191 | 199 | 183 | 183 |
| $\delta^{13}C$ | ‰ | 0.53 | 0.41 | 0.40 | 0.38 |
| $CO_3^{2-}$ ion | µmol $kg^{-1}$ | 90.9 | 86.7 | 84.8 | 88.6 |
| Salinity | Psu | 34.57 | 34.57 | 34.57 | 34.57 |
| Temperature | °C | 4.16 | 4.16 | 4.16 | 4.16 |

**Table 3.** Global mean values of the modern ocean for the sensitivity experiments above.

Second, seawater $\delta^{13}C$ can also be altered via exchange with the atmospheric $CO_2$, without any associated changes in nutrient concentrations. Isotope equilibrium of surface ocean waters with atmospheric $CO_2$ will cause higher $\delta^{13}C$ in cold surface waters, and lower $\delta^{13}C$ in warm surface waters (Broecker and Maier-Reimer 1992). The difference between the equilibration of $CO_2$ and the isotopes is that the isotopes require more time to reach equilibrium (about 10 years compared to about 1 year, depending on the depth of the mixed layer and the gas-exchange rate). Because surface waters move about and are replaced on faster timescales than this, there is no region of the ocean where surface water carbon is in complete isotopic equilibrium with the atmosphere (Broecker and Maier-Reimer 1992). To extract the effect of the gas-exchange signature from biological induced alterations, the artificial tracer ($\delta^{13}C_{as}$) could be constructed according to Broecker and Maier-Reimer (1992). If there were no air-sea exchange, the relationship between $\delta^{13}C$ and $PO_4^{3-}$ in the ocean would be

$$d^{13}\mathrm{C} - d^{13}\mathrm{C}_{\mathrm{mean}} = \frac{\Delta_{\mathrm{photo}}}{\Sigma\mathrm{CO}_{2\,\mathrm{mean}}} \cdot \frac{\mathrm{C}}{\mathrm{P}} \cdot (\mathrm{PO}_4 - \mathrm{PO}_{4\,\mathrm{mean}}). \quad (1)$$

The suffix mean denotes average ocean concentrations and $\Delta_{photo}$ and C/P describe the mean $\delta^{13}C$ in particulate organic matter and the Redfield ratio between organic carbon and phosphorus, respectively. When reasonable values are substituted ($\delta^{13}C_{mean}$ = 0.3 ‰, $\Delta_{photo}$ = -20 ‰, $\Sigma CO_{2\,mean}$ = 2200 µmol $kg^{-1}$, C/P = 128 and $PO_4^{3-}{}_{mean}$ = 2.2 µmol $kg^{-1}$), the predicted relationship between $\delta^{13}C$ and

$PO_4^{3-}$ closely matches the relationship for waters of the deep Indian and Pacific Oceans ($^{13}C$ = 2.7 - 1.1 x $PO_4^{3-}$). This is to be expected, as the effect of air-sea exchange should be constant for theses deep waters on account of the homogeneity of source waters of the deep Indian and Pacific Oceans. The degree to which air-sea exchange processes have affected the surface ocean $\delta^{13}C$ can determined by subtracting the $\delta^{13}C$ value predicted from biological cycling exclusively from the actual $\delta^{13}C$,

$$d^{13}\mathrm{Cas} = d^{13}\mathrm{C} - (2.7 - 1.1 \cdot \mathrm{PO}_4). \quad (2)$$

By definition, water with $\delta^{13}C_{as}$ of 0.0 ‰ has the same air-sea exchange signature as the mean ocean deep water. A positive value of $\delta^{13}C_{as}$ means that the water reveals more of an influence of air-sea exchange at cold temperatures and less at warmer temperatures, whereas a negative $\delta^{13}C_{as}$ value implies less $\delta^{13}C$ enrichment due to air-sea exchange than for average deep ocean water. However, this formulation will only represent the true effects of air-sea exchange if the assumptions about constant C/P ratios and constant $\delta^{13}C$ of organic material and reasonable biologically induced changes in oceanic carbon content are sufficiently accurate. For example, Antarctic surface water, where $\delta^{13}C$ of organic matter is substantially lower than in the rest of the ocean, $\delta^{13}C_{as}$ will lead to an overestimation of the effects of the air-sea exchange. For the glacial ocean, we used the same formulation according to Winguth et al. (1999), but assume the same Redfield slope as for the modern ocean,

$$d^{13}\mathrm{Cas} = d^{13}\mathrm{C} - (2.5 - 1.1 \cdot \mathrm{PO}_4). \quad (3)$$

The effect of the ocean circulation on the $\delta^{13}C$ distribution, appart from the advection of tracers, depends on the residence time of a water mass. The longer a water mass resides in the deep-sea, the more organic material degrades within it, consuming oxygen and depleting $^{13}C$. Circulation changes were accompanied with changes in the temperature and salinity which influences the solubility and dissociation constants of $CO_2$.

A further effect on the marine $\delta^{13}C$ came from the biosphere where the organic $\delta^{13}C$ is lower (about -25 ‰) than the marine $\delta^{13}C$ (about -20 ‰). Changes in the vegetation, soil composition and transport of carbon via continental fluxes to the ocean could influenced the concentration of $\delta^{13}C$. Estimations of this effect on the LGM $\delta^{13}C$ ranged from 0.3 to 0.4 ‰ (Curry et al. 1988; Duplessy et al. 1988).

## Carbon Cycle Modelling Results

### *Modern Atlantic (Control Run)*

The reference run (control run) of the carbon cycle model yielded a global primary production rate of 8.62 GtC $year^{-1}$ and a new production rate (defined as the amount of newly formed organic matter which is transferred from the surface layer into deeper layers each year and is thereby removed from the seasonal ocean-atmospheric exchange cycle) of 6.7 GtC $year^{-1}$ (see Table 2). The magnitudes of these values were within the range of results of other global biogeochemical models (e.g. Yamanaka and Tajika 1997; Marchal et al. 1998; Murnane et al. 1999). Estimates from observed data of primary and new production were difficult to compare directly with model outputs, because they included different methods for determining the various kinds of production. Estimations of the global new production ranged between 5.0 and 22.0 GtC $year^{-1}$ (Murnane et al. 1999). The preindustrial atmospheric $pCO_2$ became stationary at 281 ppm and was in good agreement with estimates from ice cores . The global mean $\delta^{13}C$ value amounted to 0.38 ‰ (see Table 3), and was slightly lower than the value of 0.50 ‰ reported by Broecker and Maier-Reimer (1992).

The simulated present-day $\delta^{13}C$ distributions along the Geochemical Ocean Section Study (GEOSECS) sections in the Western and Eastern Atlantic are shown in Figure 2. The GEOSECS data set has been corrected according to Kroopnick (1985). For the Eastern Atlantic transect, we extended the GEOSECS data set to the south using the data set of Mackensen et al. (1996). The GEOSECS transect in the Western Atlantic remained unchanged. The main features of the dif-

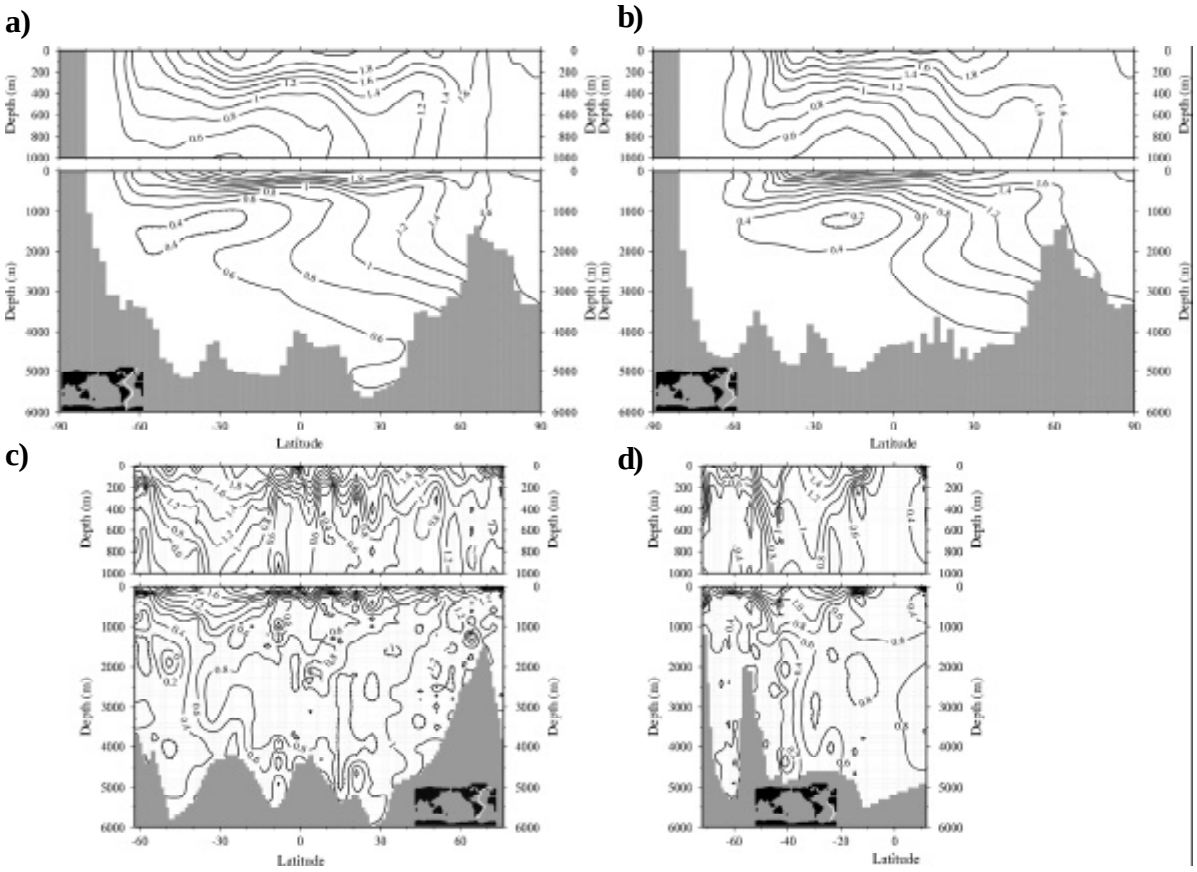


**Fig. 2.** Meridional distribution of $\delta^{13}C$ in the modern Atlantic Ocean. Contour interval is 0.2 ‰, see small panel for location of the section. **a)** and **b)** Simulated distribution in the Western and Eastern Atlantic, respectively. **c)** Observed $\delta^{13}C$ distribution in the Western Atlantic (GEOSECS), corrected according to Kroopnick (1985). **d)** GEOSECS distribution of $\delta^{13}C$ in the Eastern Atlantic. The GEOSECS transect is extended to the south according to Mackensen et al. (1996).

ferent water masses are adequately reproduced by the model. NADW and AABW can be clearly distinguished, with high and low $\delta^{13}C$ values, respectively. A shortcoming in the simulated $\delta^{13}C$ distribution was the shallower level of the NADW water mass. The core of this water mass was about at 2,500 m depth in the Western Atlantic, whereas in GEOSECS it was about 500 m deeper, but as mentioned above, this represents one model layer at this depth level. This discrepancy was primarily a result of the lower than observed meridional overturning. The simulated minimum of $\delta^{13}C$ in the Antarctic Intermediate Water (AAIW) compares well with data, but the values in the AABW seemed to be up to 0.2 ‰ higher, especially in the Western Atlantic.

In Table 4 we calculated the root mean square error between the control run and GEOSECS data for the entire Atlantic. Table 4 reveals a greater discrepancy of the simulated $\delta^{13}C$ distribution in the modern northern Atlantic compared to the south. This was a further implication for the underestimation of the simulated NADW production.

The contribution of the gas-exchange signature ($\delta^{13}C_{as}$) in the eastern Atlantic is shown in Figure 3. At the ocean surface, the contribution of the $\delta^{13}C_{as}$ signature is mainly due to the temperature dependence of the gas-exchange formulation (see Heinze et al. 1991). Cold regions like the Southern Ocean show higher $\delta^{13}C_{as}$ values than the warm waters of the equator and subtropical gyres, with mostly negative values relative to the deep-sea.

| | Control run | Experiment 1 | Experiment 2 | Experiment 3 |
|---|---|---|---|---|
| 75 °N - 60 °N | 0.53 | - | - | - |
| 60 °N - 45 °N | 0.43 | 0.28 | 0.33 | 0.27 |
| 45 °N - 30 °N | 0.36 | 0.19 | 0.51 | 0.19 |
| 30 °N - 15 °N | 0.52 | 0.25 | 0.35 | 0.25 |
| 15 °N - 0 ° | 0.42 | 0.20 | 0.61 | 0.20 |
| 0 ° - 15 °S | 0.40 | 0.12 | 0.63 | 0.12 |
| 15 °S - 30 °S | 0.29 | 0.28 | 0.82 | 0.28 |
| 30 °S - 45 °S | 0.26 | 0.26 | 0.67 | 0.26 |
| 45 °S - 60 °S | 0.33 | - | - | - |
| 60 °S - 71 °S | 0.27 | - | - | - |
| Entire Atlantic | 0.38 | 0.23 | 0.57 | 0.23 |

**Table 4.** Root mean square error between simulated $\delta^{13}C$ values for the control run, glacial experiment 1, 2, 3 and observed data in the entire Atlantic Ocean. Modern data: From GEOSECS, corrected according Kroopnick (1985) and Mackensen et al. (1996). LGM data: From Sarnthein et al. (1994) north of the equator and south of the equator, see Bickert and Mackensen this volume.

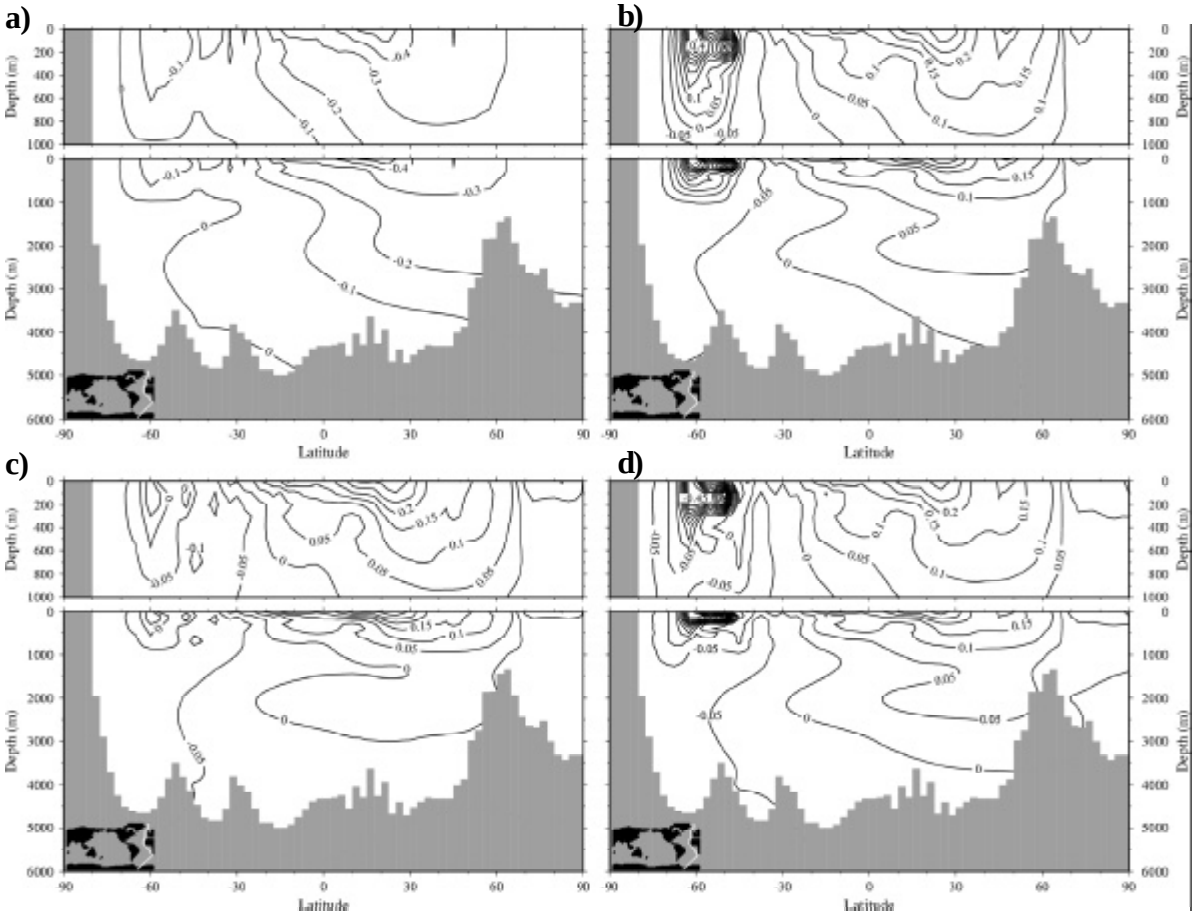


**Fig. 3.** Meridional section of the gas exchange signature ($\delta^{13}Cas$) in the Eastern Atlantic, see small panel for location of the section. **a)** Latitude-depth section of $\delta^{13}Cas$ for the control run. Contour interval is 0.1 ‰. **b)** Anomaly between glacial experiment 1 and control run. **c)** Anomaly between glacial experiment 2 and control run. **d)** Anomaly between glacial experiment 3 and control run. Contour interval for the anomalies are 0.05 ‰.

Thus the Southern Ocean surface water is enriched in $\delta^{13}C$ from the gas-exchange with the atmosphere at cold temperatures, whereas the warm water regions are reduced in $\delta^{13}C$. However, in the surface water of the Southern Ocean, upwelling of deep water ($\delta^{13}Cas$ = 0.0 ‰) influences the gas-exchange signature and the observed low $\delta^{13}C$ in organic matter would tend to overestimate the contribution of the gas-exchange signature in this area. The high $\delta^{13}Cas$ values of about 0.5 ‰ in the surface water of the Weddell Sea - according to Lynch-Stieglitz et al. (1995) - were not reproduced by the model. One reason could be the use of a constant gas-exchange rate, but Lynch-Stieglitz et al. (1995) have shown that its influence was low. It is most likely that the simulated surface $\delta^{13}C$ values were underestimated, whereas the $PO_4^{3-}$ concentration remained in the range of the observations. The deep water column in the north reflected the transport and mixing of NADW carried the gas-exchange signature to the south. The NADW should have a $\delta^{13}C_{as}$ of about -0.4 ‰ according to Broecker and Maier-Reimer (1992), whereas our simulation reached a value of about -0.2 ‰.

### *Glacial Atlantic (Experiment 1)*

To investigate the response of the $\delta^{13}C$ distribution in the Atlantic Ocean to climate change, we performed three model experiments for the glacial Atlantic. Experiment 1 used a modified temperature, salinity, circulation field and more extended ice distribution as driven by glacial ocean circulation. Experiment 2 introduced, in addition, an initial nutrient inventory which was increased by 30 %. To reduce the $pCO_2$ in the atmosphere without significant changes in the $\delta^{13}C$ values we setup an model run with a chemical glacial ocean according to Sanyal et al. (1995). As a result, experiment 1 showed a reduced new production rate of 5.9 GtC year$^{-1}$ compared to 6.7 in the control run, and the change in the global mean of $\delta^{13}C$ amounted to 0.15 ‰. The average atmospheric $pCO_2$ was lowered by 1 ppm and attains a value of 280 ppm. The differences in $\delta^{13}C$ in the Atlantic are shown in Figure 4 for the Western and in Figure 5 for the Eastern Atlantic. In the deep Atlantic, there was a reduction of 0.2 ‰ as compared to the modern state, whereas the upper ocean north of the equator showed an increase in $\delta^{13}C$. A possible cause of the simulated decrease of $\delta^{13}C$ in the deep ocean is aging of the deep water masses due to the reduced NADW formation and export to the Southern Ocean. The influence of the gas-exchange signature on the $\delta^{13}C$, due to the lower glacial temperatures, showed only minor changes in the deep water column compared to the control run (Fig. 3). Only the surface ocean is significantly affected by the air-sea exchange, especially in the Southern Ocean near the sea-ice edge. The effect of changes in the pattern of the remineralisation of organic matter on the decrease of the $\delta^{13}C$ should be minor, since the global new production is lower in this simulation.

In summary, the simulated distribution of $\delta^{13}C$ in the Atlantic Ocean showed a lowering in the $\delta^{13}C$ of 0.2 ‰ in the deep water column, which was only due to a changed thermohaline circulation field. However, the effect of this circulation on the $pCO_2$ in the atmosphere was too small to explain the concentrations measured in ice cores. This supports previous findings of Heinze et al. (1999) and Winguth et al. (1999). Therefore, we setup a model run with an intensified biological pump.

### *Glacial Atlantic (Experiment 2)*

In this experiment, we increased the initial nutrient inventory of the glacial ocean by 30 %. Together with the glacial circulation field, this yields a new production rate of 7.5 GtC year$^{-1}$. As a result, the atmospheric $pCO_2$ was reduced to 221 ppm. This approaches the observed $pCO_2$ value of approximated 200 ppm for the LGM (e.g. Barnola et al. 1987; Petit et al. 1999). The global mean $\delta^{13}C$ value is reduced to -0.47 ‰. The enhancement of the new production is accompanied by an additional reduction of the $\delta^{13}C$ in the whole water column of the Atlantic Ocean due to the remineralisation of organic matter (Fig. 6 and 7). Under these conditions, large parts of the deep water column reveal negative $\delta^{13}C$ values. The gas-exchange signature shows no significant changes compared to experiment 1, except in the upper ocean of the Southern Ocean, but this has no influences on the

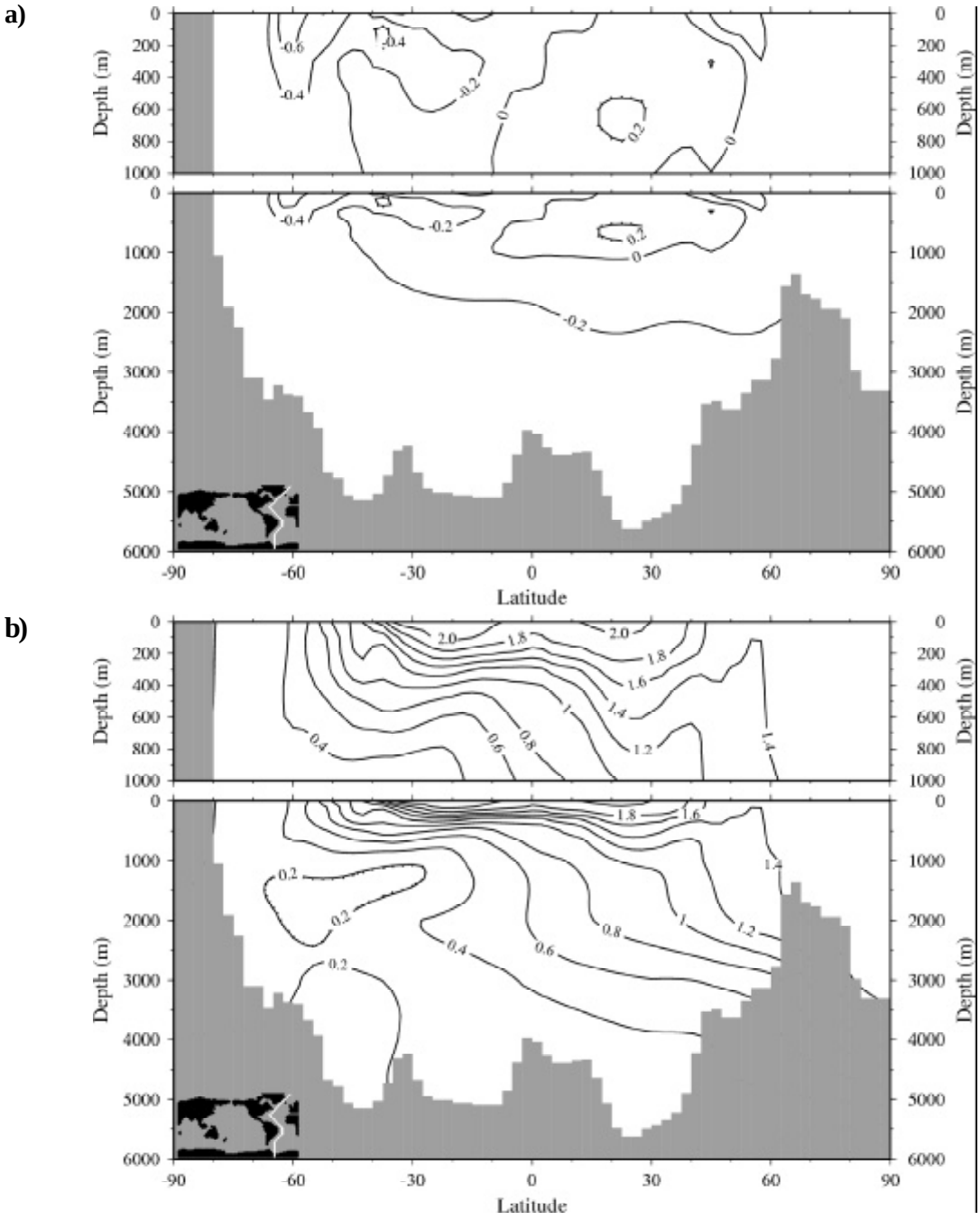


**Fig. 4.** Meridional distribution of $\delta^{13}C$ in the Western Atlantic for glacial experiment 1. Contour interval is 0.2 ‰. **a)** Anomaly between experiment 1 and control run. **b)** Simulated $\delta^{13}C$ distribution.

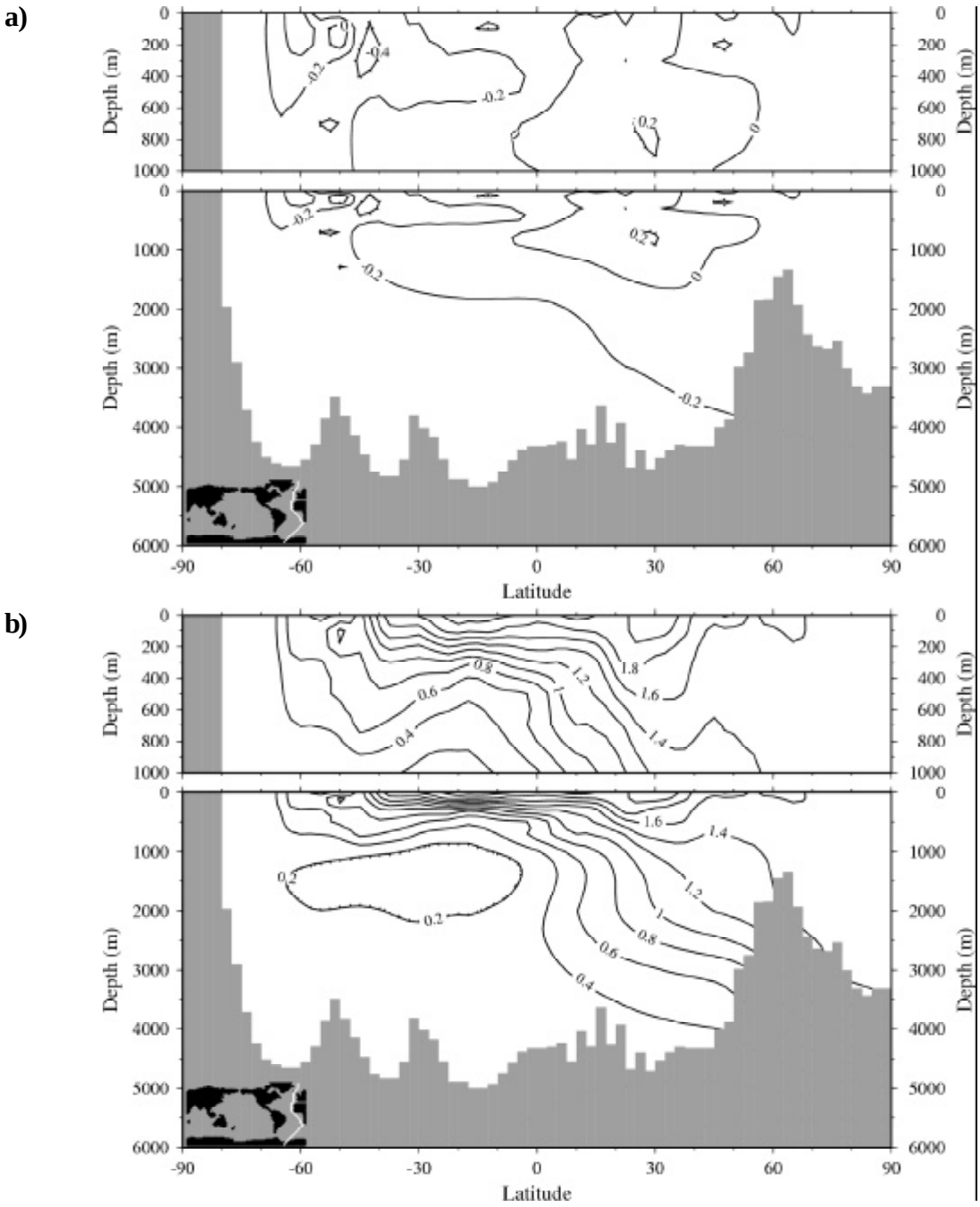


**Fig. 5.** Meridional distribution of $\delta^{13}C$ in the Eastern Atlantic for glacial experiment 1. Contour interval is 0.2 ‰. **a)** Anomaly between experiment 1 and control run. **b)** Simulated $\delta^{13}C$ distribution.

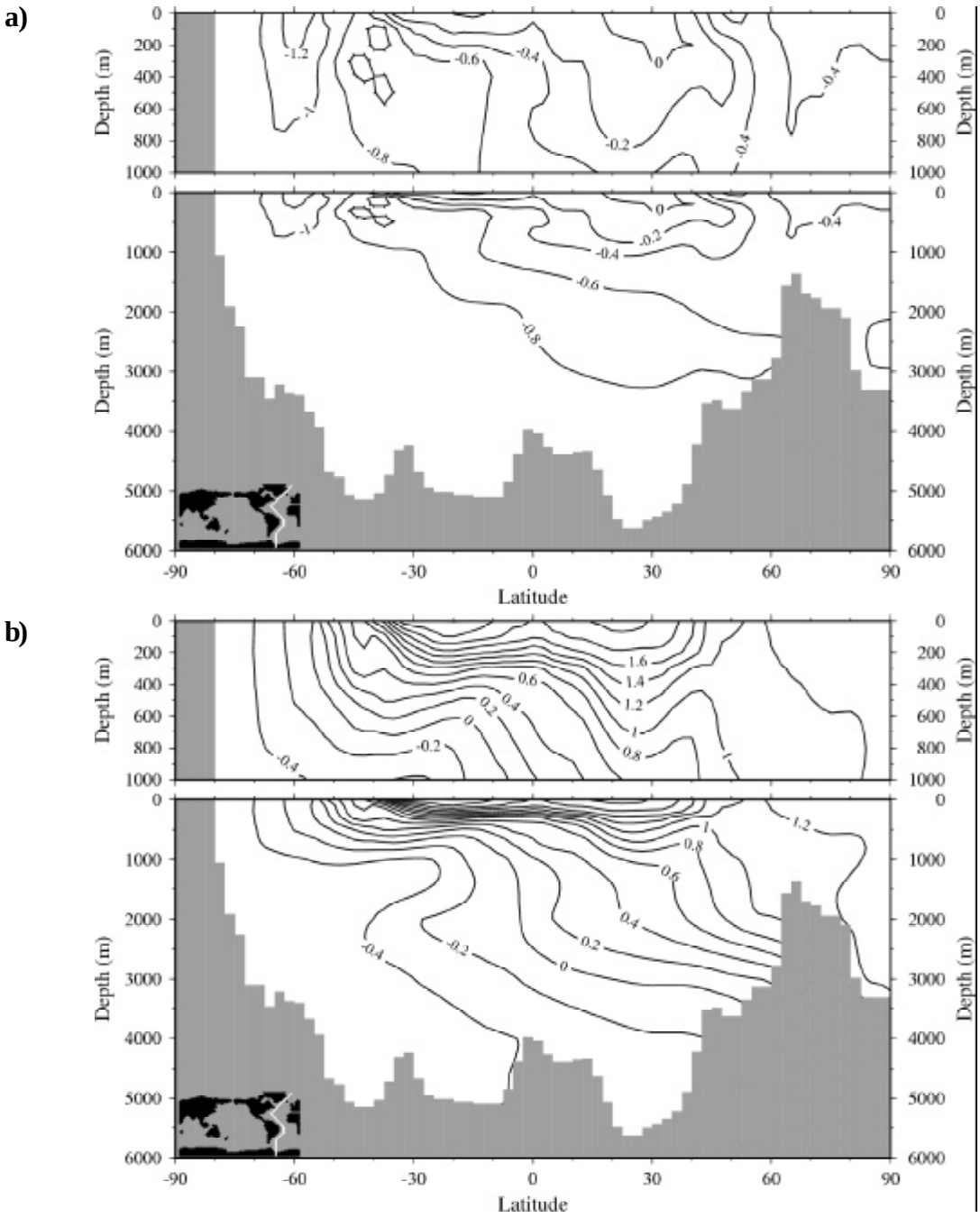


**Fig. 6.** Meridional distribution of $\delta^{13}C$ in the Western Atlantic for glacial experiment 2. Contour interval is 0.2 ‰. **a)** Anomaly between experiment 2 and control run. **b)** Simulated $\delta^{13}C$ distribution.

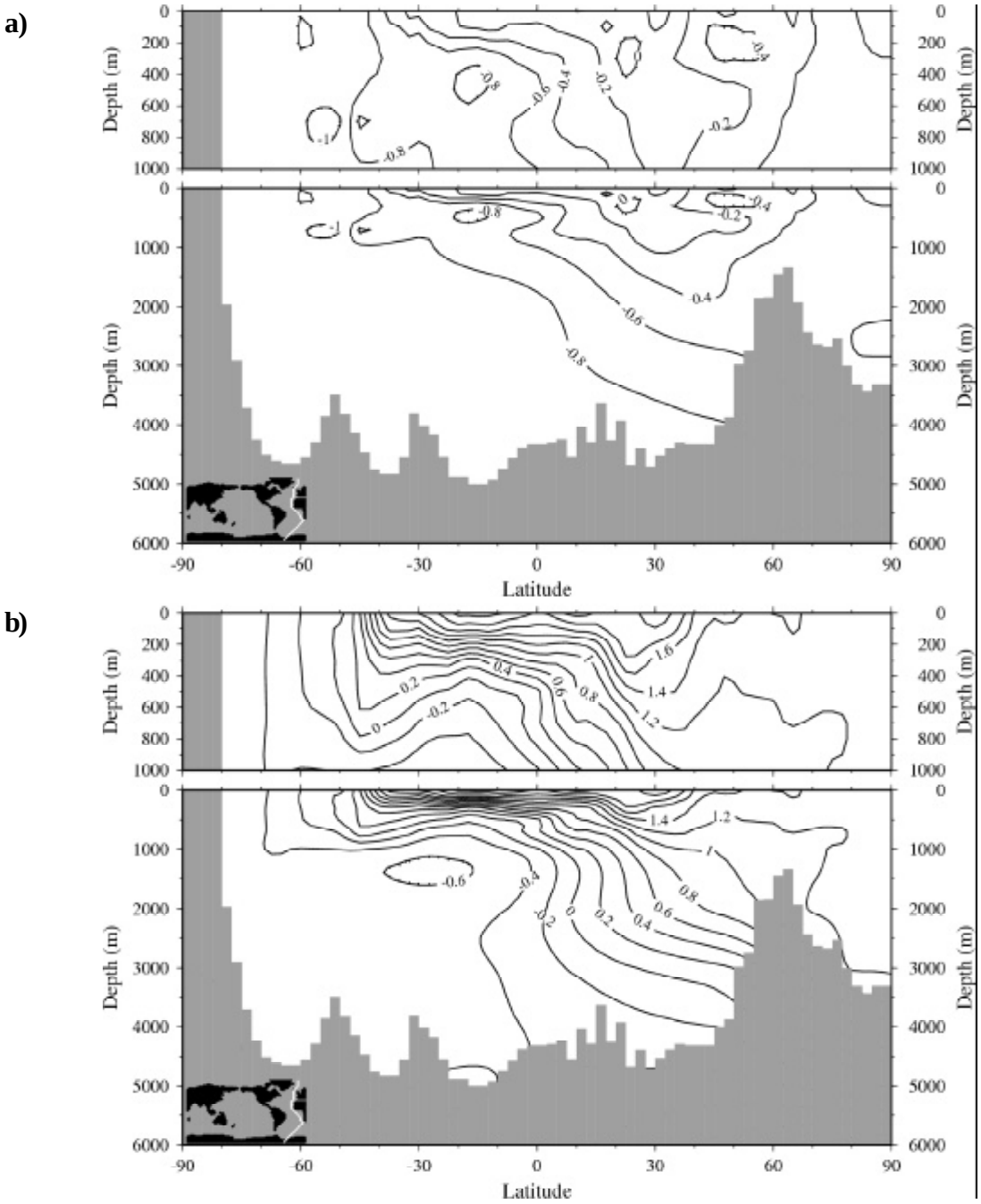


**Fig. 7.** Meridional distribution of $\delta^{13}C$ in the Eastern Atlantic for glacial experiment 2. Contour interval is 0.2 ‰. **a)** Anomaly between experiment 2 and control run. **b)** Simulated $\delta^{13}C$ distribution.

deep water column in this region (compare Fig. 3b with 3c).

### *Glacial Atlantic (Experiment 3)*

Experiment 3 was based on the observations of Sanyal et al. (1995) that the pH values of the glacial deep waters in the Atlantic and Pacific are 0.3 ±0.1 higher as compared to the Holocene period. If the observed higher glacial pH was the result of excess calcite dissolution, then $0.157 \times 10^{-3}$ moles of $CaCO_3$ must have been added to each kilogram of sea water. This corresponds to $0.161 \times 10^{-3}$ mol $l^{-1}$, if a mean density of 1.025 kg $l^{-1}$ is assumed. We translated these conditions to an increase of the initial model concentrations of 161 µmol $l^{-1}$ $\Sigma CO_2$ and 2 x 161 µequiv $l^{-1}$ alkalinity. To mirror an increase of $C_{org}$ in the sediment we halved the maximal rain ratio to 0.075.

It must be considered that this experiment does not take into account the complex interactions between the sediment and the overlying water. In this experiment we introduced the effects of these interactions according to the assumptions of Sanyal et al. (1995), because the model has only a very simple sediment module with a constant exchange rate between the bottom water and sediment layer. The new production is the same as in experiment 1, only the $CaCO_3$ production is lower because of the reduced rain ratio (from 0.15 to 0.075). The implication on the $\delta^{13}C$ distribution is minimal (Fig. 8 and 9) and the $pCO_2$ decrease to 250 ppm due to the weakening of the carbonate pump. The proposed rise in the pH value of 0.3 in the glacial deep Atlantic according to Sanyal et al. (1995) is not predicted by the model. A maximum elevation of 0.2 in the pH value is found in the northern Indic Ocean at a water depth of 1,500 m, however, in the Atlantic we only reached a maximal increase of 0.1 at about 1,000 m. The reduction of the atmospheric $pCO_2$ is purchased at the expense of a deepening of the lysocline in the glacial Atlantic, which contradicts observations that show an upward movement of the lysocline. The simulated gas-exchange signature shows roughly the same anomaly patterns as in the other experiments, with an exception in the Southern Ocean, where $\delta^{13}C_{as}$ shows a strong depression relative to the source water (Fig. 3d).

## Comparison of Model Results with Paleoclimate Data

In Figures 10 through 13 we compare the distributions of $\delta^{13}C$ in glacial simulations and in the paleoclimate records of the Western and Eastern Atlantic. A new data set of benthic stable isotopes from sediment cores in the South Atlantic (Bickert and Mackensen this volume) combined with the data of Sarnthein et al. (1994) for the eastern North Atlantic, allows a more detailed reconstruction of the glacial nutrient distribution in this region most sensitive to circulation changes. For the South Atlantic, only values of sites outside of upwelling areas have been chosen for the reconstruction of $\delta^{13}C$ distributions in the past. Several studies from different locations in the South Atlantic have shown that an additional depletion in the $\delta^{13}C$ of epibenthic foraminifer calcite occurs in areas characterized by high surface water productivity and hence high organic matter supply to the seafloor (e.g. Mackensen et al. 1993; Bickert and Wefer 1999). This depletion is most likely explained to be caused by the decay of organic matter, reducing $^{13}C/^{12}C$ ratio in the pore water, which influences to some degree the carbon isotopic composition of the *C. wuellerstorfi* shells of high-productive areas. Therefore, we removed the values of such locations prior to the model-paleodata comparison (see Bickert and Mackensen this volume, for a detailed discussion).

As a result, there is a reasonable fit of the model output of experiment 1 to the $\delta^{13}C$ distribution derived from sediment samples, when the glacial export of NADW to the Southern Ocean is reduced by 50 % and the inflow of glacial AABW is held constant (Fig. 10 and 11, Table 4). The obtained $\delta^{13}C$ pattern from the model experiment matches the paleodata within a range of ±0.2 ‰ for most of the data. Furthermore, the asymmetry between the glacial NADW distribution in the South Atlantic basins is reproduced by the coupled ocean circulation and carbon cycle model. However, some data points in the mid-depth Western Atlantic between 15° and 30° south would suggest the glacial

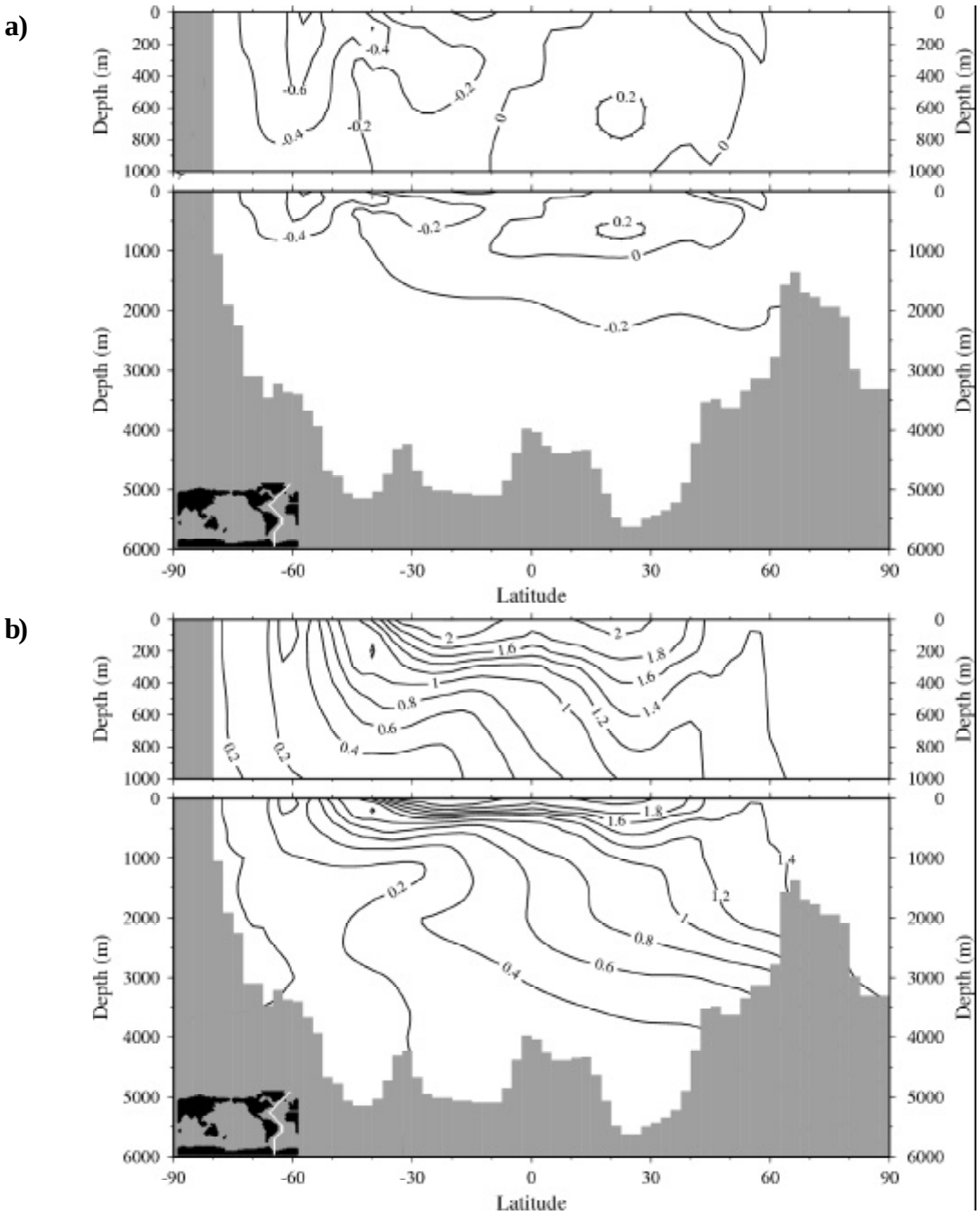


**Fig. 8.** Meridional distribution of $\delta^{13}C$ in the Western Atlantic for glacial experiment 3. Contour interval is 0.2 ‰. **a)** Anomaly between experiment 3 and control run. **b)** Simulated $\delta^{13}C$ distribution.

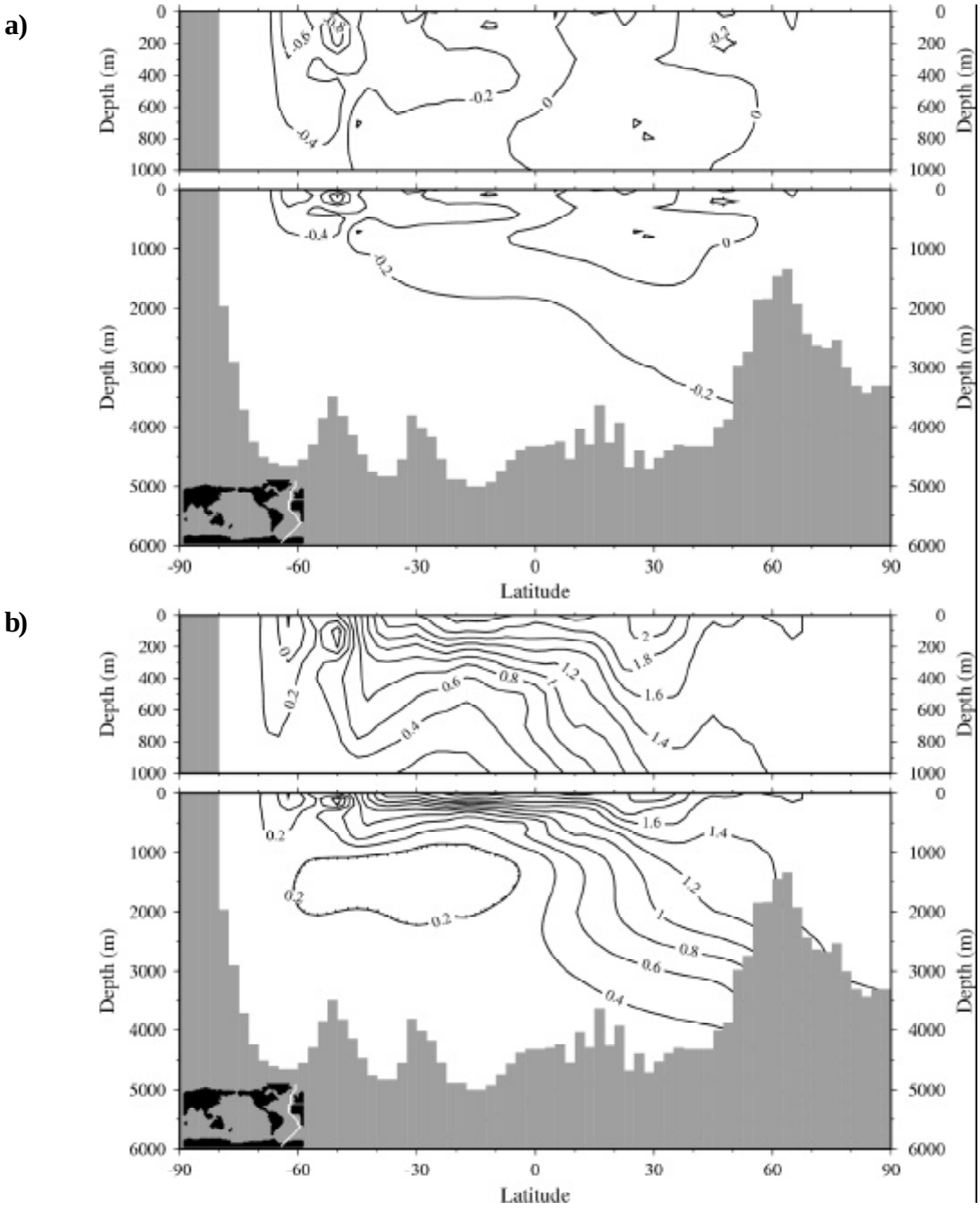


**Fig. 9.** Meridional distribution of $\delta^{13}C$ in the Eastern Atlantic for glacial experiment 3. Contour interval is 0.2 ‰. **a)** Anomaly between experiment 3 and control run. **b)** Simulated $\delta^{13}C$ distribution.

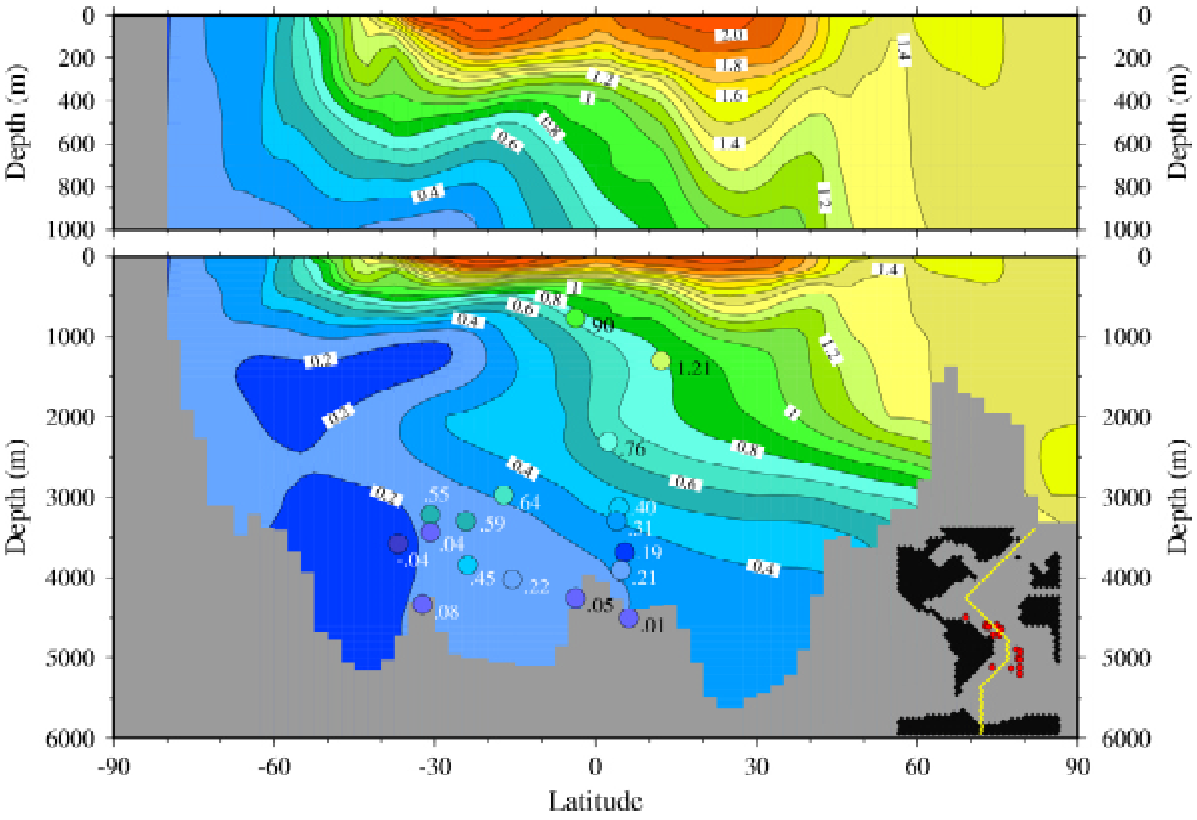


**Fig. 10.** Comparison between the glacial $\delta^{13}C$ distribution of experiment 1 and observations (data set of SFB 261) in the Western Atlantic. Contour interval is 0.1 ‰, see small panel for locations and data points. The colours of the data points (cycles) corresponds to the colour values in the simulation. If possible, the observed $\delta^{13}C$ values are written next to the corresponding data point.

NADW to extend deeper and further south than the model does. This might be related to the underestimation of the production of NADW as already discussed for the control run of the modern ocean.

The much larger differences between the model output of experiment 2 and the paleodata (Fig. 12 and 13) indicate that there is no additional increase of the nutrient inventory of the deep ocean necessary to reproduce the paleodata. From this observation we derive that no significant increase in biological pumping occurred during glacials. As a consequence, the drop-down of atmospheric $CO_2$ could not be explained by the mechanism of an intensified biologic pumping related to an enhanced export production. This is in accordance with recent observations that the export production in the glacial Southern Ocean shows no significant changes (François et al. 1997; Nürnberg et al. 1997). However, our results would even not support the recently presented hypothesis by Stephens and Keeling (2000) that the decrease in atmospheric $CO_2$ was driven by a reduced outgassing of the upwelling deep water due to an extended sea-ice in the glacial Southern Ocean. Using a box model with deep water upwelling confined to south of 55°S, they suggested that low glacial atmospheric $CO_2$ levels might result from reduced deep water ventilation associated with either year-round Antarctic sea-ice coverage, or wintertime coverage combined with ice-induced stratification during the summer. As a result, their box model reproduces 67 ppm of the observed glacial-interglacial $CO_2$ difference and is generally consistent with the additional observational constraints.

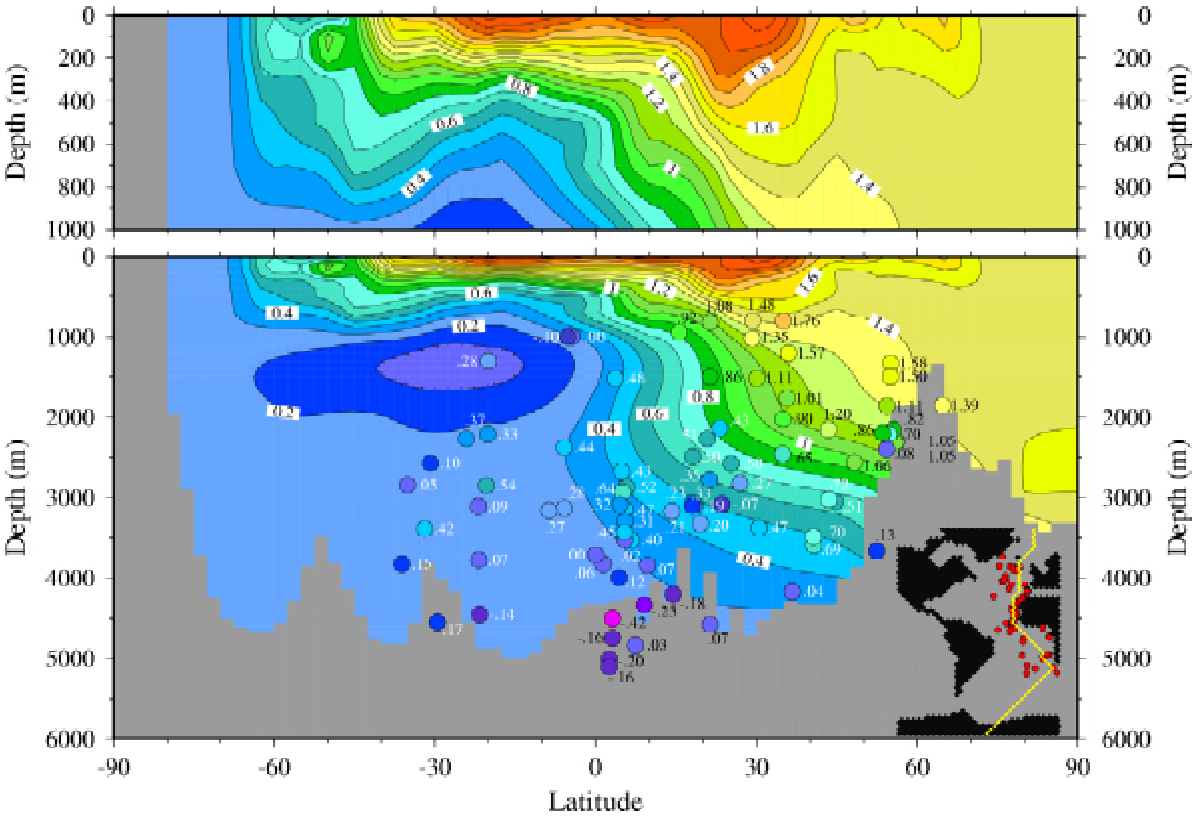


**Fig. 11.** Comparison between the glacial $\delta^{13}C$ distribution of experiment 1 and observations (data set of SFB 261 and Sarnthein et al. 1994) in the Eastern Atlantic. Contour interval is 0.1 ‰, see small panel for locations and data points. The colours of the data points (cycles) corresponds to the colour values in the simulation. If possible, the observed $\delta^{13}C$ values are written next to the corresponding data point.

Figure 14 shows the $pCO_2$ difference between ocean and atmosphere for our control run and for the glacial experiment 1 as well as the anomaly between both simulations. Negative values indicate that the ocean is a sink for atmospheric $CO_2$ and positive values indicate that the ocean is a $CO_2$ source. In both simulations the Southern Ocean represents a $CO_2$ sink.

In Table 5 we used the same area-weighted zones for the average $\Delta pCO_2$ according to Takahashi et al. (1997). For the control run the Southern Ocean represented a strong $CO_2$ sink and the equatorial region a strong source. The simulated source and sink $\Delta pCO_2$ pattern is comparable to Takahashi et al. (1997). Quantitative differences between simulations and observations are in the high latitudes of both hemispheres and primarily due to the fact that the observations are normalized to the year 1990 and the data coverage in the Southern Ocean is scarce. On the other side, the control run represented the preindustrial ocean. The simulated strong $CO_2$ sink in the Southern Ocean is supported by the observations of Schlitzer (2002) who predicted a significant stronger export production in this region as satellite observations indicated. This should result in a stronger $CO_2$ input to the surface ocean. In the Atlantic sector of the Southern Ocean this sink seems to be stronger in the glacial run compared to the control run. The minimum value in this region amounts to -80 ppm, whereas in the control run it amounts to -60 ppm. However, the area of the $pCO_2$ sink is reduced compared to the modern conditions due to the extended sea-ice coverage. This is also taken from

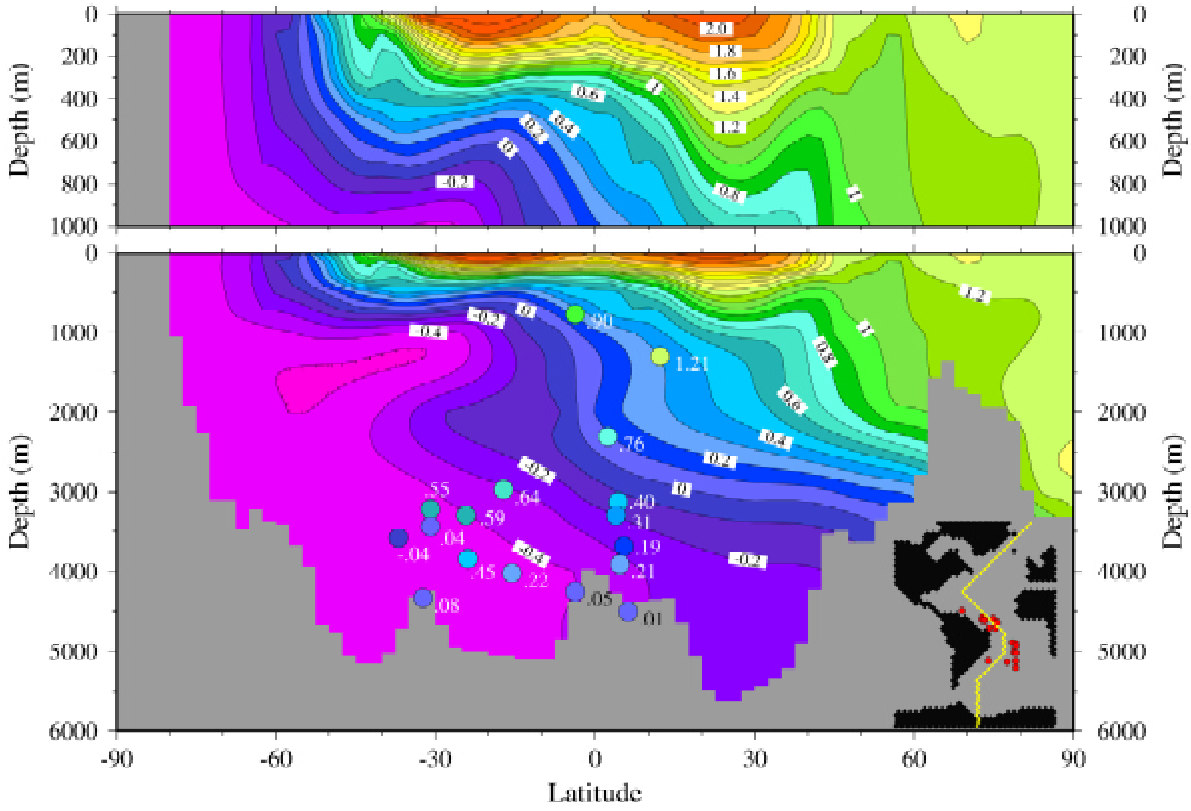


**Fig. 12.** Comparison between the glacial $\delta^{13}C$ distribution of experiment 2 and observations (data set of SFB 261) in the Western Atlantic. Contour interval is 0.1 ‰, see small panel for locations and data points. The colours of the data points (cycles) corresponds to the colour values in the simulation. If possible, the observed $\delta^{13}C$ values are written next to the corresponding data point.

Table 5 where the average $\Delta pCO_2$ values show a reduction in the $CO_2$ sink between 50°S and 90°S due to the sea-ice expansion compared to the control run. An intensification is predicted in the zone between 14°S and 50°S. Together with the biological new production which is only slightly stronger in the vicinity of the sea-ice edge in this region, the contribution to lowering the global mean atmospheric $pCO_2$ appears to be small. Based on our model simulations the extended sea-ice cover in the LGM could not have been responsible for the strong reduction of the global atmospheric $CO_2$.

The reason for the obvious discrepancy between the results of Keeling and Stephens (2001) and our model output might be that box models and general circulation models (GCM) show a strong different behaviour to changes in the high latitudes (Archer et al. 2000b). As an example the GCM simulation of Archer et al. (2000a) under conditions of a more efficient nutrient utilization in the glacial Southern Ocean as a result of a higher iron supply shows no sufficient atmospheric $CO_2$ reduction, whereas box models (see references in Archer et al. 2000b) reaches the glacial $CO_2$ concentration. This different behaviour of the models to changes in high latitudes was discussed in Archer et al. (2000b) and they concluded that box models overestimate high latitude sensitivity of the real ocean. This uncertainty should be examined in more detail.

The dramatic changes in the circulation and associated exchange processes in the Southern Ocean as proposed by Toggweiler (1999) are always accompanied with changes in the tempera-

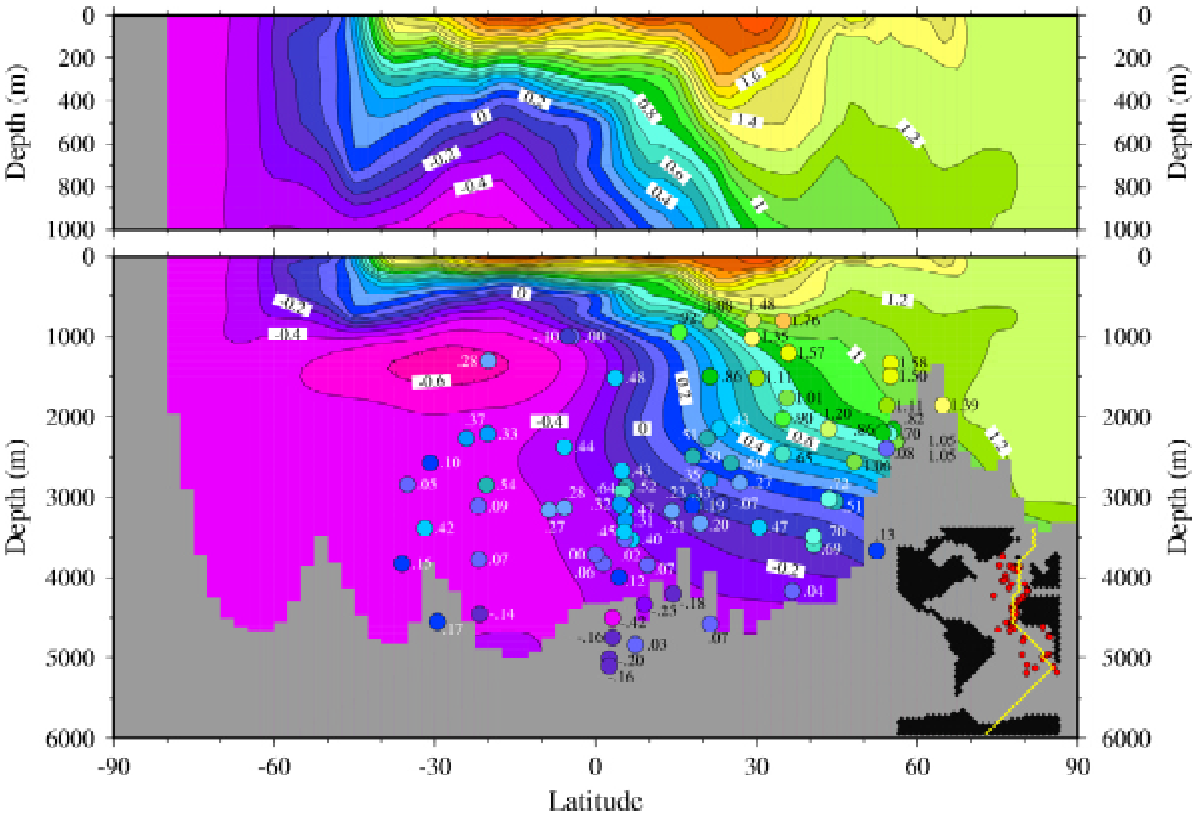


**Fig. 13.** Comparison between the glacial $\delta^{13}C$ distribution of experiment 2 and observations (data set of SFB 261 and Sarnthein et al. 1994) in the Eastern Atlantic. Contour interval is 0.1 ‰, see small panel for locations and data points. The colours of the data points (cycles) corresponds to the colour values in the simulation. If possible, the observed $\delta^{13}C$ values are written next to the corresponding data point.

| Latitude zone | Control run | Experiment 1 | Experiment 2 | Experiment 3 |
|---|---|---|---|---|
| 90 °N - 50 °N | -23.86 | -10.55 | -8.62 | -9.76 |
| 50 °N - 14 °N | -3.50 | -6.67 | -5.61 | -6.15 |
| 14 °N - 14 °S | +27.64 | +23.88 | +20.61 | +22.26 |
| 14 °S - 50 °S | -4.18 | -10.62 | -9.30 | -9.91 |
| 50 °S - 90 °S | -32.60 | -10.22 | -7.55 | -8.87 |
| Global mean | -0.24 | +0.06 | +0.24 | +0.16 |

**Table 5.** Global annual mean values of sea-air $pCO_2$-difference ($\Delta pCO_2$, in ppm) for the control run and three glacial experiments for five latitude zones (area-weighted averages). The five latitude belts were selected according to Takahashi et al. (1997).

ture and salinity. Such rearrangements in the water column required, in particular, a change in the salinity that is unfortunately poorly documented for a few locations in the glacial Southern Ocean.

Ultimately, the influence of increased sea-ice in the Southern Ocean and/or a northward shift of glacial wind field on the reduction of the atmospheric $CO_2$ concentration, as was suggested by Elderfield and Rickaby (2000) and Sigman and Boyle (2000), is related to the different behaviour of the two model types. Winguth et al. (1999) have shown that an increasing glacial wind in the high

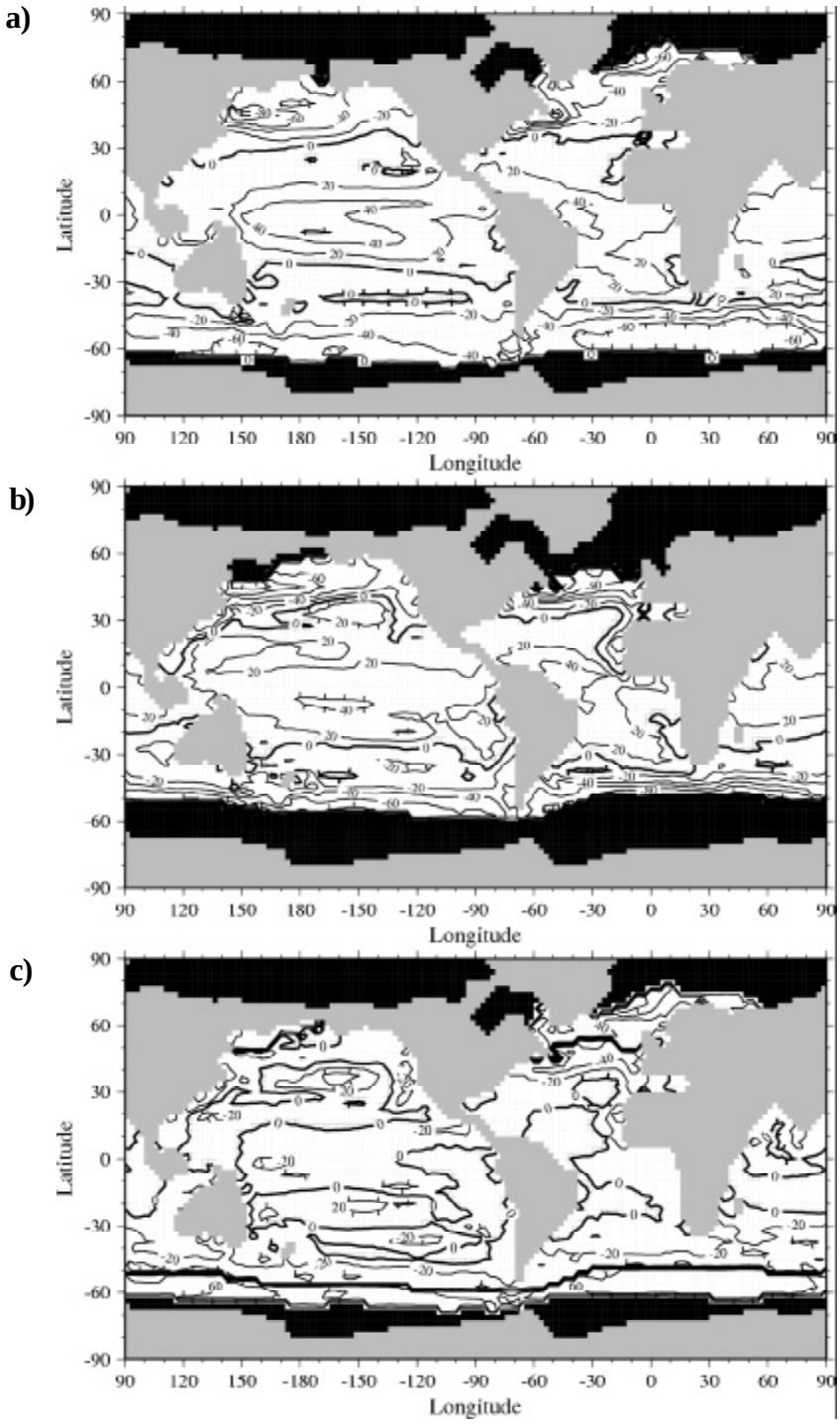


**Fig. 14.** Annual mean sea-air difference in the $CO_2$ partial pressure ($\Delta pCO_2$). Contour interval is 20 ppm. Positive values indicate that the ocean is a source for atmospheric $CO_2$, negative values indicate $CO_2$ sinks. **a)** Horizontal distribution of $\Delta pCO_2$ for the control run. **b)** Distribution of $\Delta pCO_2$ for the glacial experiment 1. **c)** Difference between experiment 1 and control run. In the two upper panels, black filled areas denote the simulated annual mean sea-ice distribution.

southern latitudes has no significant effect on the $\delta^{13}C$ pattern and the atmospheric $pCO_2$.

In our opinion, the complex mechanism of carbonate compensation represents a common way of reducing the atmospheric $pCO_2$, without producing a strong reduction of the $\delta^{13}C$. However, Archer et al. (2000a) have shown in a model simulation which included a complex sediment module that this process works in the right direction, but violates other paleoevidences from sediments, e.g. changes in the depth of the lysocline and the $CaCO_3$ distribution on the seafloor.

In experiment 3, we mimiced the mechanism of the carbonate compensation according to Sanyal et al. (1995) and could reduce the atmospheric $pCO_2$ to 250 ppm with a $\delta^{13}C$ pattern like in experiment 1 (see Figs. 8, 9 and Table 4). However, the advantage of the $pCO_2$ reduction in the atmosphere and the reasonable reproduction of the $\delta^{13}C$ distribution is obtained at the expense of carbonate distributions which are not in agreement with observations. For example, the glacial lysocline in the Western Atlantic is deeper (500 to 1,000 m) as compared to the modern situation, whereas observation indicated a rise of the glacial lysocline (Henrich et al. this volume). The estimated pH reduction according to Sanyal et al. (1995) in the glacial Atlantic was not reproduced by the model.

Figure 15 shows another comparison between modelled results and observations in terms of standard deviation and correlation coefficient.

After interpolating modelled data to the observed data levels, the standard deviation and the correlation coefficient were calculated for both data sets (model experiments and observations). These data pairs were transferred as polar coordinates into a scatter diagram according to Taylor (Gates et al. 1998; Taylor 2001). The procedure of the conversion of the value pair in the Taylor diagram was done in three steps:

1. Normalization of the standard deviation of the model simulation and observation was defined as $\sigma_{norm} = \sigma^2_{model} \times \sigma^{-2}_{observation}$.
2. The polar angle, $\alpha$, was calculated as follows: $\alpha = \arccos r$. The parameter r denotes the correlation coefficient.
3. The determination of the values for the x- and y-axis (the polar coordinates) was calculated by using the equations $x = \sigma_{norm} x \cos \alpha$ and $y = \sigma_{norm} x \sin \alpha$.

The Taylor diagram showed the degree of correspondence between simulated and observed $\delta^{13}C$ fields in the Atlantic Ocean. By definition, all observations showed a normalized standard deviation of 1 and an angle of zero degrees (i.e. the correlation coefficient is equal to 1). This point was accepted as reference point which determines the locality of the various observed data sets used in this diagram and always have the same position. The distance of the simulated tracer point from the origin of the coordinate system is equal to the standard deviation (normalized by the observed standard deviation), whereas the distance from the reference point (observations) is equivalent to the rms (root mean square) pattern difference between the observed and modeled data fields (again normalized by the observed standard deviation). The cosine of the polar angle corresponds to the correlation between the simulated and observed data sets. Thus, a model that is relatively accurate would lie near the dashed arc (indicating it had the correct variance) and close to the observed reference point indicating a small rms error and a high correlation coefficient. The outer circular arc in Figure 15 describes the correlation coefficient. In Figure 15 a), we show the comparison between the model simulations (control run, glacial experiment 1 and 2. Please note that experiment 3 shows the same position as experiment 1 and remains unmentioned in the legend of Figure 15) and the observed data sets (modern: GEOSECS, glacial: Sarnthein et al. 1994). The glacial modeled $\delta^{13}C$ fields are more closely resembled the observation fields (in terms von standard deviation, correlation coefficient and rms error) than the modern modeled $\delta^{13}C$ field. The reason may probably be attributed to the previous finding of low NADW production. The glacial simulation of experiment 2 substantially presents a better agreement between the observed $\delta^{13}C$ pattern of Sarnthein et al. (1994) than the simulation of experiment 1 (and experiment 3).

As shown in Figure 15 b), we combined the observed $\delta^{13}C$ data set of GEOSECS with the data of Mackensen et al. (1996). The observed glacial data set include data of Sarnthein et al. (1994), relating to the north of the equator, otherwise, $\delta^{13}C$

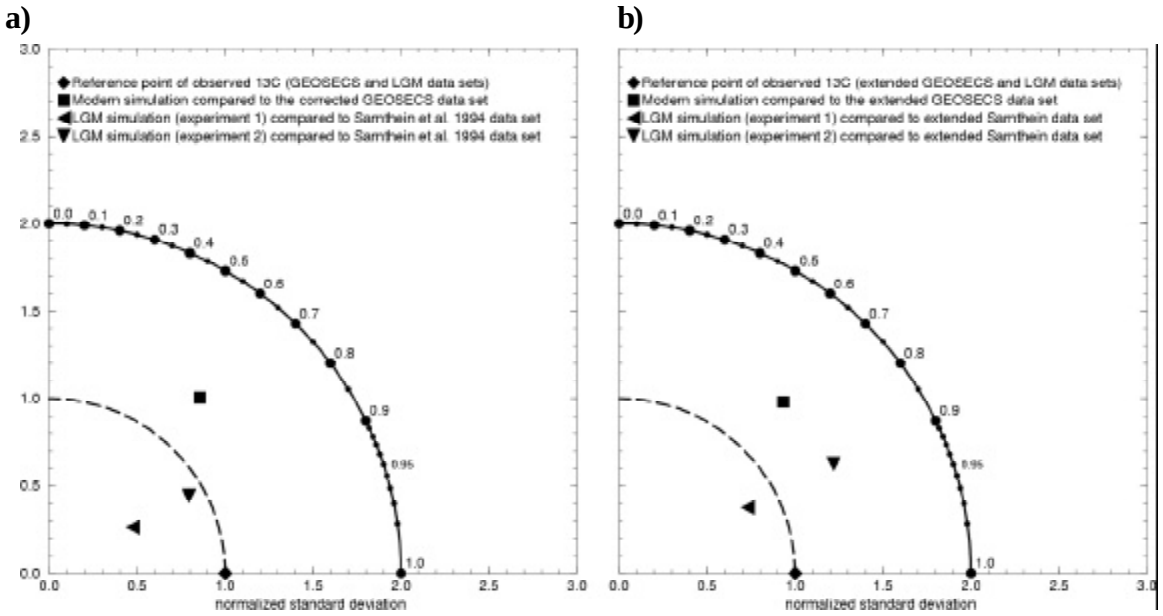


**Fig. 15.** Comparison between simulated $\delta^{13}C$ pattern with observed $\delta^{13}C$ in the entire Atlantic Ocean. The graphical representation is according to Taylor (Gates et al.1998, Taylor 2001), see text for details. **a)** Simulated $\delta^{13}C$ pattern for the control and the both glacial runs (experiment 1 and 2) in comparison with the GEOSECS observations and the data of Sarnthein et al. (1994). Note that experiment 3 in this diagram shows the same position as experiment 1 and remains unmentioned in the legend. **b)** The same as left, but for extended data sets. For the modern case the GEOSECS data are replenished to the south according to Mackensen et al. (1996). For the comparison with the glacial simulations, we used the data of Sarnthein et al. (1994) north of the equator, otherwise the SFB 261 data set is used.

data measured by the research program of SFB 261 were used. For the modern situation, this led to a slightly improved conformity with these data sets at least as far as the correlation coefficient was concerned. The situation of the glacial simulation showed an opposite behaviour in the $\delta^{13}C$ pattern between experiment 1 (and 3) and 2. The simulation in experiment 1 (and 3) now reveals a better conformity with the observation than could be archieved in experiment 2.

## Summary and Conclusions

The new paleodata set of the LGM shows - especially in the South Atlantic - that the reduction of $\delta^{13}C$ in the deep water column is less pronounced than previously assumed. In particular, the Western Atlantic shows no negative $\delta^{13}C$ values. This corresponds favourably with the glacial simulation of experiment 1, in which only the thermohaline circulation conditions have changed. As compared to the modern ocean, the data in the glacial Eastern Atlantic show generally very low $\delta^{13}C$ concentrations in the deep water column between 20°N and the equator. In the Eastern Atlantic, the simulated $\delta^{13}C$ concentrations correspond well to the observations. In general, deviations are in the range of ±0.2 ‰, with an exception around 20°N where the model produced 0.4 ‰ higher concentrations as compared to the observations. However, in spite of the good correlation between glacial simulation and observation the reduction of the atmospheric $CO_2$ partial pressure is too low. Thus, the model could reproduce the observed $\delta^{13}C$ pattern, but it was not able to simulate the glacial/interglacial $pCO_2$ change of about 80 ppm. The distribution of the new production in the Atlantic, not shown, indicated a slight increase in the productivity in the ice free polar regions, whereas the tropical and subtropical ocean showed no significant changes com-

pared to the modern distribution. This simulated pattern is supported by observations that new or export production showed no significant changes in the glacial Southern Ocean (François et al. 1997; Nürnberg et al. 1997) and oligothrophic open ocean regions (Sarnthein et al. 1988; Mix 1989). However, evidences of higher paleoproductivity were observed in the glacial Atlantic, particularly in the eastern boundary upwelling regions (Sarnthein et al. 1988; Schneider et al. 1996) and in the equatorial zones (Mix 1989; Lyle et al. 1992; Schneider et al. 1996). A decrease of paleoproductivity was found in the Artic Ocean (Sarnthein et al. 1988; Schubert and Stein 1996; Knies and Stein 1998).

In model experiment 2 (implications of a stronger biological pump), simulated $\delta^{13}C$ concentrations revealed that the reduction of carbon isotopes was highly overestimated as compared to the observations in the whole Atlantic. However, with respect to the atmospheric $CO_2$ concentration, the decrease amounted to 60 ppm as compared to the control run and was in relative good accordance with observations from ice cores. The export production in this simulation showed a strong increase in the whole ice free ocean. This was supported by observations made at the glacial subantarctic Atlantic Ocean (Kumar et al. 1995), equatorial Atlantic (Sarnthein et al. 1988; Mix 1989; Lyle et al. 1992) and upwelling regions of the eastern Atlantic (Sarnthein et al. 1988; Schneider et al. 1996).

Experiment 3 displayed a relative strong reduction of the glacial atmospheric $pCO_2$, in combination with a good reproduction of the $\delta^{13}C$ distribution in the Atlantic. However, the result does not agree with observations of changed lysoclines. An improved model performance could be archieved by accounting for the following considerations:

- As mention above, the physical ocean model showed a too shallow southward extension of the NADW. A higher vertical resolution of the model could result in a better resolution of the various main water masses.
- In the carbon cycle model, the $\delta^{13}C$ of particulate organic matter was calculated with a constant carbon isotope fractionation factor of –20 ‰. However, observations from the Southern Ocean showed values lower than –30 ‰ in $\delta^{13}C$ of organic matter in the surface water. These low organic carbon isotope values were not reproduced by the model. Rau et al. (1991) attribute the low $\delta^{13}C$ of organic material in this region to the increased pool of aqueous $CO_2$ in these cold waters. A $CO_2$-dependent carbon isotope fractionation could possibly correct this discrepancy between simulation and oberservation in the Southern Ocean.
- A more complex production formulation including more different biological species could also improve model performance. However, the functional relationships between the various species are not well understood yet.
- A more complex sediment module should be included which would enhance the performance in the carbonate chemistry.
- A module of the land biosphere should be included which would supply more information on the effect of the marine carbon isotopes.

However, these recommendations are only helpful, if the functional relationships are sufficiently known, ideally, on a global or basin wide scale.

We conclude on the base of our model simulations that no additional increase of the deep ocean's nutrient inventory is necessary to reproduce the $\delta^{13}C$ distribution in the glacial Atlantic, which indicate no significant increase in biological pumping during the LGM. This would exclude all hypotheses that involve changes in the nutrient inventory and/or Redfield ratios to explain the atmospheric glacial-interglacial $CO_2$ reduction. Our results would rather support other scenarios for the decrease of glacial atmospheric $pCO_2$, such as the mechanism of carbonate compensation.

## Acknowledgments

The models LSG and HAMOCC have been developed and put at our disposal by the Max-Plank-Institut für Meteorologie. Special thanks go to Andreas Manschke for his technical support. The careful comments of A. Winguth and R. Zahn were considerably helpful in improving the manuscript. We kindly acknowledge financial support from Deutsche Forschungsgemeinschaft (Sonderforschungsbereich 261). Data are available under www.pangaea.de/Projects/SFB261.

## References


Anderson LA, Sarmiento JL (1994) Redfield ratios of remineralization determined by nutrient data analysis. Glob Biogeochem Cycl 8: 65-80

Arakawa A, Lamb VR (1977) Computational design of basic dynamical process of the UCLA general circulation model. Meth Comput Phys 16: 173-283

Archer D, Winguth A, Lea D, Mahowald N (2000a) What Caused the Glacial/Interglacial Atmospheric $pCO_2$ Cycles? Rev Geophys 38: 159-189

Archer DE, Eshel G, Winguth A, Broecker WS, Pierrehumbert R, Tobis M, Jacob R (2000b) Atmospheric $pCO_2$ sensitivity to the biological pump in the ocean. Glob Biogeochem Cycl 14: 1219-1230

Bacastow R, Maier-Reimer E (1990) Ocean-circulation model of the carbon cycle. Clim Dyn 4:95-125

Barnola JM, Raynaud D, Korotkevich YS, Lorius C (1987) Vostok ice core provides 160,000-year record of atmospheric $CO_2$. Nature 329: 408-414

Bickert T, Wefer G (1999) South Atlantic and benthic foraminifer $\delta^{13}C$-deviations: Implications for reconstructing the Late Quaternary deep-water circulation. Deep-Sea Res 46: 437-452

Broecker WS, Maier-Reimer E (1992) The influence of air and sea exchange on the carbon isotope distribution in the sea. Glob Biogeochem Cycl 6: 315-320

Broecker WS, Henderson GM (1998) The sequence of events surrounding Termination II and their implications for the cause of glacial-interglacial $CO_2$ changes. Paleoceanography 13: 352-364

Curry WB, Duplessy JC, Labeyrie LD, ShackletonPNJ (1988) Changes in the distribution of $\delta^{13}C$ of Deep Water $CO_2$ between the Last Glaciation and the Holocene. Paleoceanography 3: 317-341

Duplessy JC, Shackleton NJ, Fairbanks RG, Labeyrie L, Oppo D, Kallel N (1988) Deepwater source variations during the last climatic cycle and their impact on the global deepwater circulation. Paleoceanography 3: 343-360

Elderfield H, Rickaby REM (2000) Oceanic Cd/P ratio and nutrient utilization in the glacial Southern Ocean. Nature 405: 305-310

François R, Altabet MA, Yu EF, Sigman DM, Bacon MP, Frank M, Bohrmann G, Bareille G, Labeyrie LD (1997) Contribution of Southern Ocean surface-water stratification to low atmospheric $CO_2$ concentrations during the last glacial period. Nature 389: 929-935

Friedli H, Lötscher H, Oeschger H, Siegenthaler U, Stauffer B (1986) Ice core record of the $^{13}C/^{12}C$ ratio of atmospheric $CO_2$ in the past two centuries. Nature 324: 237-238

Gates WL, Boyle JS, Covey CC, Dease CG, Doutriaux CM, Drach RS, Fiorino M, Gleckler PJ, Hnilo JJ, Marlais SM, Phillips TJ, Potter GL, Santer BD, Sperber KR, Taylor KE, Williams DN (1998) An Overview of the Results of the Atmospheric Model Intercomparison Project (AMIP). Report 45, The Program for Climate Model Diagnosis and Intercomparison, Livermore, http://www-pcmdi.llnl.gov/pcmdi/pubs/ab45.html

Heinze C, Maier-Reimer E, Winn K (1991) Glacial $pCO_2$ reduction by the world ocean: Experiments with the Hamburg Carbon Cycle Model. Paleoceanography 6: 395-430

Heinze C, Maier-Reimer E, Winguth AME, Archer D (1999) A global oceanic sediment model for long-term climate studies. Glob Biogeochem Cycl 13:221-250

Johns TC, Carnell RE, Crossley JF, Gregory JM, Mitchell JFB, Senior CA, Tett SFB, Wood RA (1997) The second Hadley Centre coupled ocean- atmosphere GCM: Model description, spinup and validation. Clim Dyn 13: 103-134

Keeling RF, Stephens BB (2001) Antarctic sea ice and the control of Pleistocene climate instability. Paleoceanography 16: 112-131 and (corrections) 330-334

Knies J, Stein R (1998) New aspects of organic carbon deposition and its paleoceanographic implications along the northern Barents Sea margin during the last 30,000 years. Paleoceanography 13: 384-394

Kroopnick PM (1985) The distribution of $^{13}C$ of $CO_2$ in the world oceans. Deep-Sea Res 32: 57-84

Kumar N, Anderson RF, Mortlock RA, Froelich PN, Kubik P, Dittrich- Nannen B, Suter M (1995) Increased biological productivity and export production in the glacial Southern Ocean. Nature 378:675-680

Leonard BP (1979) A stable and accurate convective modeling procedure based on quadratic upstream interpolation. Comp Meth Appl Mech Eng 19:59-98

Levitus S, Russell B, Boyer TP (1994) World Ocean Atlas 1994. Volume 3: Salinity. Technical report, National Oceanic and Atmospheric Administration, Washington DC

Lorenz S, Grieger B, Helbig P, Herterich K (1996) Investigating the sensitivity of the atmospheric general circulation model ECHAM 3 to paleoclimatic boundary conditions. Geol Rundsch 85: 513-524

Lyle MW, Prahl FG, Sparrow MA (1992) Upwelling and productivity changes inferred from a temperature record in the central equatorial Pacific. Nature 355: 812-815

Lynch-Stieglitz J, Stocker T, Broecker WS, Fairbanks RG

(1995) The influence of air-sea exchange on the isotopic composition of oceanic carbon: Observations and modeling. Glob Biogeochem Cycl 9: 653-665

Mackensen A, Hubberten HW, Bickert T, Fischer G, Fütterer DK (1993) The $\delta^{13}C$ in benthic foraminiferal tests of *Fontbotia Wuellerstorfi* (Schwager) relativ to the $\delta^{13}C$ of dissolved inorganic carbon in Southern Ocean Deep Water: Implications for glacial ocean circulation models. Paleoceanography 8: 587-610

Mackensen A, Hubberten HW, Scheele N, Schlitzer R (1996) Decoupling of $\delta^{13}CTCO_2$ and phosphate in Recent Weddel Sea deep and bottom water: Implications for glacial Southern Ocean paleoceanography. Paleoceanography 11: 203-215

Maier-Reimer E, Hasselmann K (1987) Transport and storage of $CO_2$ in the ocean - an inorganic ocean-circulation carbon cycle model. Clim Dyn 2: 63-90

Maier-Reimer E, Mikolajewicz U, Hasselmann K (1993) Mean circulation of the Hamburg LSG OGCM and Its Sensitivity to the Thermohaline Surface Forcing. J Phys Oceanogr 23: 731-757

Marchal O, Stocker TF, Joos F (1998) Impact of oceanic reorganizations on the ocean carbon cycle and atmospheric carbon dioxide content. Paleoceanography 13: 225-244

Mix AC (1989) Influence of productivity variations on long-term atmospheric $CO_2$. Nature 337: 541-544

Murnane RJ, Sarmiento JL, Le Quéré C (1999) Spatial distribution of air-sea $CO_2$ fluxes and the interhemispheric transport of carbon by the oceans. Glob Biogeochem Cycl 13: 287-305

Nürnberg CC, Bohrmann G, Schlüter M, Frank M (1997) Barium accumulation in the Atlantic sector of the Southern Ocean: Results from 190,000-year records. Paleoceanography 12: 594-603

Petit JR, Jouzel J, Raynaud D, Barkov NI, Barnola JM, Basile I, Bender M, Chappellaz J, Davis M, Delaygue G, Delmotte M, Kotlyakov VM, Legrand M, Lipenkov VY, Lorius C, Pépin L, Ritz C, Saltzman E, Stievenard M (1999) Climate and atmospheric history of the past 420,000 years from the Vostok ice core, Antarctica. Nature 399: 429-436

Rau GH, Takahashi T, Des Marais DJ, Sullivan CW (1991) Particulate organic matter $\delta^{13}C$ variations across the Drake Passage. J Geophys Res 96: 15131-15135

Rau GH, Riebesell U, Wolf-Gladrow D (1997) $CO_2$aq-dependent photosynthetic $^{13}C$ fractionation in the ocean: A model versus measurements. Glob Biogeochem Cycl 11: 267-278

Sanyal A, Hemming NG, Hanson GN, Broecker WS (1995) Evidence for a higher ph in the glacial ocean from boron isotopes in foraminifera. Nature 373: 234-236

Sarnthein M, Winn K, Duplessy JC, Fontugne MR (1988) Global variations of surface ocean productivity in low and mid latitudes: Influence on $CO_2$ reservoirs of the deep ocean and atmosphere during the last 21,000 years. Paleoceanography 3: 361-399

Sarnthein M, Winn K, Jung SJA, Duplessy JC, Labeyrie L, Erlenkeuser H, Ganssen G (1994) Changes in east Atlantic deepwater circulation over the last 30,000 years: Eight time slice reconstructions. Paleoceanography 9: 209-267

Schäfer-Neth C, Paul A (2001) Circulation of the Glacial Atlantic: A Synthesis of Global and Regional Modeling. In: Schäfer P, Ritzrau W, Schlüter M, Thiede J (eds) The Northern North Atlantic: A Changing Enviroment. Springer, Berlin, pp 441-462

Schlitzer R (2002) Carbon export fluxes in the Southerrn Ocean: Results from inverse modelling and compaison with satellite-based eastimates. Deep-Sea Res 49: 1623-1644

Schmitz WJ (1995) On the Interbasin-Scale Thermohaline Circulation. Rev Geophys 33: 151-173

Schneider RR, Müller PJ, Ruhland G, Meinecke G, Schmidt H, Wefer G (1996) Late quaternary surface temperatures and productivity in the east-equatorial south atlantic: Response to changes in trademonsoon wind forcing and surface water advection. In: Wefer G, Berger W, Siedler G, Webb DJ (eds) The South Atlantic: Present and Past Circulation. Springer, Berlin, pp 527-551

Schubert CJ, Stein R (1996) Deposition of organic carbon in Arctic Ocean sediments: Terrigenous supply versus marine productivity. Org Geochem 24: 421-436

Shea DJ, Trenberth KE, Reynolds RW (1990) A global monthly sea surface temperature climatology. NCAR Technical Note NCAR/TN 345, NCAR, Boulder, Colorado

Sigman DM, Boyle EA (2000) Glacial/interglacial variations in atmospheric carbon dioxide. Nature 407: 859-869

Stephens BB, Keeling RF (2000) The influence of Antarctic sea ice on glacial-interglacial $CO_2$ variations. Nature 404: 171-174

Suess E (1980) Particulate organic carbon flux in the oceans-surface productivity and oxygen utilization. Nature 288: 260-263

Takahashi T, Feely RA, Weiss R, Wanninkhof R, Chipman DW, Sutherland SC, Takahashi TT (1997) Global air-sea flux of $CO_2$: An estimate based on measurements of air-sea $pCO_2$ difference. Proc Natl Acad Sci 94: 8292-8299

Taylor KE (2001) Summarizing multiple aspects of model

performance in a single diagram. J Geophys Res 106: 7183-7192

Toggweiler JR (1999) Variation of atmospheric $CO_2$ by ventilation of the ocean's deepest water. Paleoceanography 14: 571-588

Weinelt M, Sarnthein M, Pflaumann U, Schulz H, Jung S, Erlenkeuser H (1996) Ice-free Nordic Seas during the Last Glacial Maximum? Potential sites of deepwater formation. Paleoclimatology 1: 283-309

Winguth AME, Archer D, Duplessy JC, Maier-Reimer E, Mikolajewicz U (1999) Sensitivity of paleonutrient tracer distributions and deep-sea circulation to glacial boundary conditions. Paleoceanography 14: 304-323

Yamanaka Y, Tajika E (1996) The role of the vertical fluxes of particulate organic matter and calcite in the oceanic carbon cycle: Studies using an ocean biogeochemical general circulation model. Glob Biogeochem Cycl 10: 361-382

Yamanaka Y, Tajika E (1997) Role of dissolved organic matter in the marine biogeochemical cycle: Studies using an ocean biogeochemical general circulation model. Glob Biogeochem Cycl 11: 599-612

Yu EF, François R, Bacon MP (1996) Similar rates of modern and last-glacial ocean thermohaline circulation inferred from radiochemical data. Nature 379: 689-694